UNIVERSITY OF BLIDA 1
INSTITUTE OF AERONAUTICS AND SPACE STUDIES

Modelling, Design and Construction of a Quadcopter Platform

A Thesis Submitted by

Abdellah HASSAINE

In Partial Fulfilment of the Requirements for

The Degree of Master in Aeronautics
Option: Structure

Under the Supervision of

Dr. Ahemd CHGRANI

Jury Members

Dr. **Mohamed KHODJET-KESBA**	UNIVERSITY OF BLIDA 1
Prof. **Ahmed BEKHTI**	UNIVERSITY OF BLIDA 1

September 2020


بسم الله الرحمن الرحيم

Acknowledgment

After finishing this work, with the help of Sublime God, I would first like to thank my father and mother for their continuous support and help and for everything they gave to me.

I would also like to thank my supervisor Prof. Ahmed CHEGRANI for his valuable help and precious suggestions during the development of this work.

My special thanks are extended to all my family, friends, and everyone who helped me in some manner to reach this modest objective in my life.

و الحمد لله رب العالمين

Abdellah HASSAINE

September 2020, Algiers

Abstract

Multicopters are increasingly common, but one category of these aircrafts is more popular in academia and hobbyist communities, that is quadcopters. In this thesis we treat the general aspects related to this aircraft from early history to recent projects and diverse uses. We also address in detail the dynamical modelling to give the equations of motions. However the main contribution of this work was the design of a quadcopter platform, where we performed a static structural analysis to study the stress and deformation state under an extreme condition (high vertical acceleration) which proved the airframe to be safe from rupture. We also studied the effect of changing the orthotropic orientations of the material and compared it with the adopted configuration. Finally, a real model was constructed to be ready for use in controlled flights.

Keywords: Airframe design; CAD; Dynamic modelling; FEM; Multicopter; Quadcopter; UAV.

ملخص

طائرات المولتيكوبتَر شائعة بتزايد، لكنَّ صنفًا من هذه الطائرات منتشر أكثر في الأوساط الأكاديمية و أوساط الهواة، إنه طائرات الكوادكوبتَر. في هذه الأطروحة نعالج النواحي العامة المتصلة بهذه الطائرة بدءًا من أوائل تاريخها وصولاً إلى التصاميم الحديثة و الاستعمالات المتعددة، نتناول أيضا النمذجة الديناميكية على نحو مفصل حتى نقدم معادلات الحركة. مع هذا فالإسهام الرئيسي لهذا العمل هو تصميم مِنصة كوادكوبتَر، حيث قمنا بعمل تحليل سكوني بُنيَوي لدراسة حالة الإجهاد و التَّشَوُّه تحت ظروف شديدة (تسارع شاقولي عالٍ) وهو ما بَيَّن سلامة الهيكل من الإنكسار. بحثنا أيضا في نتيجة تغْيِيرِ الإتجاهات الأورثُوتروبِية للمادة و قارنا ذلك مع الترتيب المتّخَذ. أخيرا، قمنا بصنع نموذج فِعلي ليكون جاهزا للاستعمال في التحليق المُسيَّر.

الكلمات المفتاحية : تصميم الهيكل؛ تصميم مدعم بالحاسوب؛ نمذجة ديناميكية؛ تحليل العناصر المنتهية؛ مولتيكوبتر؛ كوادكوبتر، طائرة غير مأهولة.

Résumé

Les multirotors sont de plus en plus répandus, mais une catégorie particulière est plus connue dans le milieu académique et chez les amateurs: ce sont les quadrirotors. Dans ce mémoire, nous traitons les aspects généraux de cet aéronef en commençant de leurs premières années d'apparition jusqu'aux projets récents et leurs diverses utilisations. Nous avons aussi abordé en détail la modélisation dynamique pour donner les équations de mouvement. Cependant la contribution principale de ce travail est la conception d'une plateforme de quadrirotor, où nous avons fait une analyse statique structurelle pour étudier l'état de contrainte et de déformation dans une condition extrême, soit une grande accélération verticale, ce qui a prouvé la sécurité contre la rupture. Nous avons aussi étudié les résultats de changement des directions orthotropes du matériau et les comparé avec la configuration adoptée. Finalement, nous avons abouti à la construction d'un model réel prêt à être utilisé dans des vols contrôlés.

Mots clés : Conception de plateforme; CAO; Modélisation dynamique; MEF, Multirotor; Quadrotor; Drone.

Contents

Acknowledgment iii

Abstract iv

Contents vii

List of symbols x

List of abbreviations xii

List of figures xiii

List of tables xv

General introduction 1

1 STATE-OF-THE-ART TECHNOLOGY AND KNOWLEDGE 2

1.1 History of quadcopters 3

1.1.1 Dormancy period (Before 1990) 3

1.1.2 Growing period (1990-2005) 5

1.1.3 Development period (2005-2010) 6

1.1.4 Activity period (2010-2013) 7

1.1.5 Booming period (2013-present) 7

1.2 Classification of quadcopters 9

1.3 Regulations and rules 11

1.3.1 Flight restriction zones and airspace use limitations 12

1.3.2 Operational limitations 14

1.3.3 Registration and piloting requirements 15

1.4 Applications and uses 15

1.4.1 In civil domain 16

1.4.1.1 Agriculture 16

1.4.1.2 Forestry 18

1.4.1.3 Search and rescue and disaster relief 19

1.4.1.4 Logistics and transport Systems 20

1.4.1.5 Infrastructure 21

1.4.1.6 Entrainment and Media 21

1.4.2 In non-civil domain 22

1.4.2.1 Military applications 22

1.4.2.2 Law enforcement and surveillance 22

1.5 Notable recent models 23
1.5.1 DJI Mavic series 23
1.5.2 Parrot AR.Drone series 24
1.5.3 Donecle Drone 25
1.5.4 Airbus Skyways drone 26
1.5.5 Ehang 184 27

2 BASICS AND DYNAMICS OF QUADCOPTERS 28

2.1 Description of a quadcopter 29

2.2 Airframe configurations 30

2.3 Control and movements of a quadricopter 31

2.4 Coordinate frames of reference 32
2.4.1 Earth frame 32
2.4.2 Body frame 32

2.5 Transfer between the frames of reference 34
2.5.1 Euler angles 34
2.5.2 Direction cosines matrix 36
2.5.3 Quaternions 36
2.5.4 Remarks on transformations of reference frames 39

2.6 System modeling 39
2.6.1 Simplifying assumptions 40
2.6.2 The Euler-Lagrange formalism 40

3 DESIGN OF THE QUADCOPTER PLATFORM 45

3.1 The design considerations 46

3.2 Case study: the design of the OS4 46
3.2.1 Mass 48
3.2.2 Geometry 48
3.2.3 Propulsion Group 49

3.3 The design of the quadcopter airframe 49
3.3.1 Numerical modelling and simulation 49
3.3.1.1 Material properties definition 50
3.3.1.2 Geometry creation 53
3.3.1.3 Boundary conditions 54
3.3.1.4 Meshing 55
3.3.2 Results 56
3.3.3 Effect of fibres orientation 59

3.3.4 Discussion of results and conclusion 62

3.4 Difficulties encountered during the design 63

4 CONSTRUCTION OF THE QUADCOPTER PLATFORM 64

4.1 Material 65

4.2 Main frame 65

4.3 The arms 67

4.4 Landing gear 68

4.5 Assembling and finishing 69

Appendix A 70

A.1 Euler angles 70

A.2 Aircraft angular rates and Euler rates 72

Conclusion and perspectives 73

BIBLIOGRAPHY 74

List of symbols

C_r	Relative change
$\boldsymbol{D}$	Transformation matrix that transforms angular rates vector to Euler angles vector (3×3)
E_i	Modulus of elasticity in the direction indicated by the subscript
$\mathrm{F_e}$	Earth reference frame
$\mathrm{F_b}$	Aircraft-body reference frame
$\widehat{\boldsymbol{F}}$	Total thrust vector (3×1)
$\boldsymbol{F_\xi}$	Translational force applied to the rotorcraft (3×1)
$\boldsymbol{g}$	Gravity acceleration vector (3×1)
G_{ij}	Modulus of rigidity in the plan indicated by the subscript
I	Cross-section moment of inertia of the quadcopter's arm
$\boldsymbol{I}$	Constant inertia matrix of the quadcopter (3×3)
$\boldsymbol{J}$	Inertia matrix expressed in terms of the generalized coordinates η (3×3)
τ_{Mi}	Couple produced by motor Mi
$\boldsymbol{\tau}$	Generalized moments applied to the rotorcraft (3×1)
f_i	Thrust force produced by the motor Mi
w_i	Angular speed of the motor Mi
k	Proportionality factor that links w_i To f_i
ℓ	Distance from the motors to the centre of gravity
L, R, T	Orthotropic directions of the wood
L	Lagrangian function
$\boldsymbol{L}$	Direction cosines matrix (3×3)
T	Kinetic energy
U	Potential energy

m	Masse of the aircraft
$\boldsymbol{q}$	Quaternion (4×1)
$\boldsymbol{q}$	Generalized coordinates of the rotorcraft (6×1)
$\boldsymbol{Q}$	Orthotropic material stiffness matrix (3×3)
$\boldsymbol{R}_a^b$	Transformation matrix that transforms from a reference frame denoted by *a* to a reference frame denoted by *b* (3×3)
s	Span of the aircraft
ν_{ij}	Poisson's ratio for an extensional stress in *j* direction
δ	Deflection of the arm
$\boldsymbol{\eta}$	Generalised coordinates attitude vector (3×1)
ψ	Yaw angle
θ	Pitch angle
ϕ	Roll angle
$\dot{\boldsymbol{\eta}}$	Generalized velocities vector (3×1)
$\boldsymbol{\Omega}$	Angular rates vector (3×1)
p	Roll angular rate
q	Pitch angular rate
r	Yaw angular rate
$\boldsymbol{\xi}$	Position generalised coordinates vector (3×1)

Note

Scalars are denoted by lightface characters, e.g.:

$$a, b, c, E, G, \nu$$

Vectors are denoted by boldface lower-case characters, e.g.:

$$\boldsymbol{a}, \boldsymbol{b}, \boldsymbol{c}$$

Matrices are denoted by boldface upper-case characters, e.g.:

$$\boldsymbol{A}, \boldsymbol{B}, \boldsymbol{C}$$

List of abbreviations

CCW	CounterClockWise
CG	Centre of Gravity
CW	ClockWise
DCM	Direction cosines matrix
DOF	Degree Of Freedom
FEM	Finite Elements Method
IMU	Inertial Measurement Unit
LOS	Line Of Sight
MEMS	Micro-Electro-Mechanical System
MTOW	Maximum Take-Off Weight
NDVI	Normalized Difference Vegetation Index
UAV	Unmanned Aerial Vehicle
VTOL	Vertical Take-Off and Landing

List of figures

Figure 1.1 Drawing of the Oehmichen No. 2 (left). Top view of De Bothezat helicopter 'Flying Octopus' as depicted in a US Patent in 1930 (Right).
Figure 1.2 Microdrone MD4-200, Professional quadcopter with + Configuration.
Figure 1.3 Evolution of papers published on drones from 2009 to 2018.
Figure 1.4 Classification according to weight.
Figure 1.5 Classification according to aerodynamic flight principle.
Figure 1.6 Posted sign banning drones at a mountain trail, USA.
Figure 1.7 Limit distance for drone flights near airports for a group of countries.
Figure 1.8 Poster warning people not to fly drones near wildfires.
Figure 1.9 Normal operators are required to maintain direct eyesight of the drone
Figure 1.10 Resolution comparison between a satellite NDVI (left) and a drone NDVI (right), the two shots were for the same day.
Figure 1.11 Drone imagery with digital post-treatment reveals individual trees locations and heights, each colour refers to a definite species.
Figure 1.12 Drone delivery of a life vest (in red) for two stranded individuals in a river, USA.
Figure 1.13 RGB (left) and TIR (right) images taken from the drone showing the same scene for a search and rescue scenario. The volunteer hiding in rocks is very difficult to discern in the RGB image but appears as a bright source in the TIR image.
Figure 1.14 Mavic Pro, the first model in the DJI Mavic series.
Figure 1.15 Illustration of the compact package of the DJI Mavic Mini.
Figure 1.16 Parrot AR. Drone 2.0 equipped with its protective indoor hull.
Figure 1.17 Donecle drone inspecting autonomously an AirFrance aircraft.
Figure 1.18 Airbus Skyways delivery drone.
Figure 1.19 Ehang 184, autonomous manned quadcopter for air transport uses.
Figure 2.1 Rotation directions of the quadcopter propellers
Figure 2.2 Propulsion configurations: tractor (top left), pusher (top right), and co-axial (bottom).
Figure 2.3 Fuselage configurations from left to right: X configuration, + configuration, and H configuration.

Figure 2.4 Body frame and Earth frame.

Figure 2.5 Euler sequence of rotations used in aerospace.

Figure 2.6 Definition of the movements and axes.

Figure 3.1 The design method flowchart of the OS4.

Figure 3.2 Mass distribution of the OS4.

Figure 3.3 Geometry of the OS4.

Figure 3.4 The three orthotropic axes of wood material.

Figure 3.5 Entering the values of the stiffness matrix in the program.

Figure 3.6 Dimensions of the central square (mm).

Figure 3.7 Assembled quadcopter and the joint type.

Figure 3.8 Boundary conditions of the quadcopter.

Figure 3.9 Boundary conditions of the isolated arm.

Figure 3.10 Mesh, orthogonal quality (left), and skewness (right).

Figure 3.11 Total deformation of the quadcopter arm (mm).

Figure 3.12 Equivalent von-Mises stress of the quadcopter arm (MPa).

Figure 3.13 Total deformation for fibre orientations b and c (mm).

Figure 3.14 Equivalent von-Mises stress for fibre orientations b and c (MPa).

Figure 3.15 Comparison of deformation values for the three fibre orientations (mm).

Figure 3.16 Comparison of stress values for the three fibre orientations (MPa).

Figure 4.1 Main frame block.

Figure 4.2 Pilot holes and pilot drill bit.

Figure 4.3 Holes that allow material cutting.

Figure 4.4 Central square after finishing.

Figure 4.5 Arms of the quadcopter.

Figure 4.6 Landing gear.

Figure 4.7 Attaching by glue.

Figure 4.8 Final quadcopter.

List of tables

Table 1.1 A number of open-source autopilot projects.

Table 1.2 Notable quadcopter models of the last development period.

Table 3.1 Values of elastics constants of the chosen wood species.

Table 3.2 Mesh principal proprieties.

Table 3.3 Average and max values of deformation and stress for different fibres orientations.

General introduction

Quadcopters are a category of vertical takeoff and landing (VTOL) aircrafts which have four motors and can carry payloads such as sensors and deliveries. They are popular and widely used in many domains. The main objective of this thesis is to design and build a quadcopter platform to be used for remotely-controlled flights.

The structure of this thesis is organized into 4 chapters. The first chapter deals with the generalities of quadcopters, it shows the development of these aircrafts and how they are classified amongst other aircrafts. We also presented the rules that regulate their use and then their most notable applications. In the end, a number of modern projects for different purposes was showed, in order to cover their wide spectrum of uses.

Chapter II deals with the technical aspects of quadcopters, it describes the basic configurations, the aircraft movements, the coordinate frames and the existing methods to transform between these frames. These concepts are the base for the derivation of the equations of motion, which is the final point of this chapter.

Chapter III is about the design of the quadcopter platform. We did a static structural analysis using Ansys to analyse the stress and deformation fields. We also investigated the orthotropic proprieties of the material and the effect of changing fibres orientations and how that will compare to the actual stress and deformation. In chapter IV we realised the model with a detailed demonstration of constriction and assembling.

1 State-Of-The-Art Technology And Knowledge

Chapter 1 Introduction

Quadcopters are very unique machines, they feature an extensive history, exceptional characteristics and widespread use. In this first chapter we will tackle this subject from the beginning until recent years, and although this aircrafts have great technical and technological capabilities, they have passed numerous development stages to reach their actual state of the art. We will also review the legal frameworks that regulate the use of these machines and we will explore the range of uses that spreads through various civil applications and non-civil applications. And finally, we will see some chosen models which contain the most recent technologies.

This chapter aims to answer the following question:

Quadcopters: How and why?

1.1 History of quadcopters

Quadcopters are not a new configuration, they have passed numerous development stages since the beginning of aviation in the 1900s. These machines are considered a member of the family of multicopters, which are in their turn a part of the larger family of aircrafts. Unlike the majority of quadcopters of today, first quadcopters were designed to be manned aircrafts and needed a sufficient amount of power to take off, which couldn't be supplied by the primitive motors of the time. Quan Quan [1] divides the development of quadrotors into 5 periods: dormancy period (before 1990), growing period (1990–2005), development period (2005–2010), activity period (2010–2013), and booming period (2013–present).

1.1.1 Dormancy period (Before 1990)

Quadcopters were among the first vertical take-off and landing vehicles (VTOLs). As early as 1907 in France, 4 years after the first successful flight, Breguet Brothers with Charles Richet built the Breguet-Richet Gyroplane No. 1, a quadcopter with an uncovered open steel framework with a powerplant at the centre. Radiating from the central structure were four wire-braced tubular steel arms, each bearing a superimposed pair of four-bladed rotors. However, it was not a free flight. It had to be steadied by a man stationed at the extremity of each of the four arms supporting the rotors – but not contributing in lift - as this primitive helicopter lacked any way to control its flight .It cannot, therefore, take the credit for being the first helicopter to make a free flight, but it was the first manned machine to raise itself vertically (only to 1.5m), by means of a rotating-wing system of lift.

Still in France, in 1920, Etienne Oemichen, an electrical engineer, also began experimenting with rotating-wing designs. His first model failed to lift from the ground. However, after some calculations and redesigns, his second aircraft the Oehmichen No. 2, depicted in figure 1.1 (Helicopters and Other Rotorcraft since 1907, Munson) proved to be the first stable quadcopter. It had 4 rotors and 8 propellers, all driven by a single engine. He first flew it in 1922 and in 1923 he broke the existing record for helicopter flight with a distance of 525 m. In 1924 he made a flight of 1 km around a closed circuit. The VTOL was then born [1] [2].

The army also had an interest in VTOL machines. In 1921, George De Bothezat and Ivan Jerome, both refugees from the Russian Revolution, were hired to develop one for the

US Army Air Corps. Their quadcopter, named the 'Flying Octopus' and shown in Figure 1.1 (US Army patent), was designed to take a payload of three people in addition to one pilot and was supposed to reach an altitude of one hundred meters, but the result was that it only managed to lift five meters and required a favourable wind to achieve forward flight. Since these early designs suffered from poor engine performance and could only reach a couple of meters high, not much improvement was done to the quadcopter design during the following three decades [1].

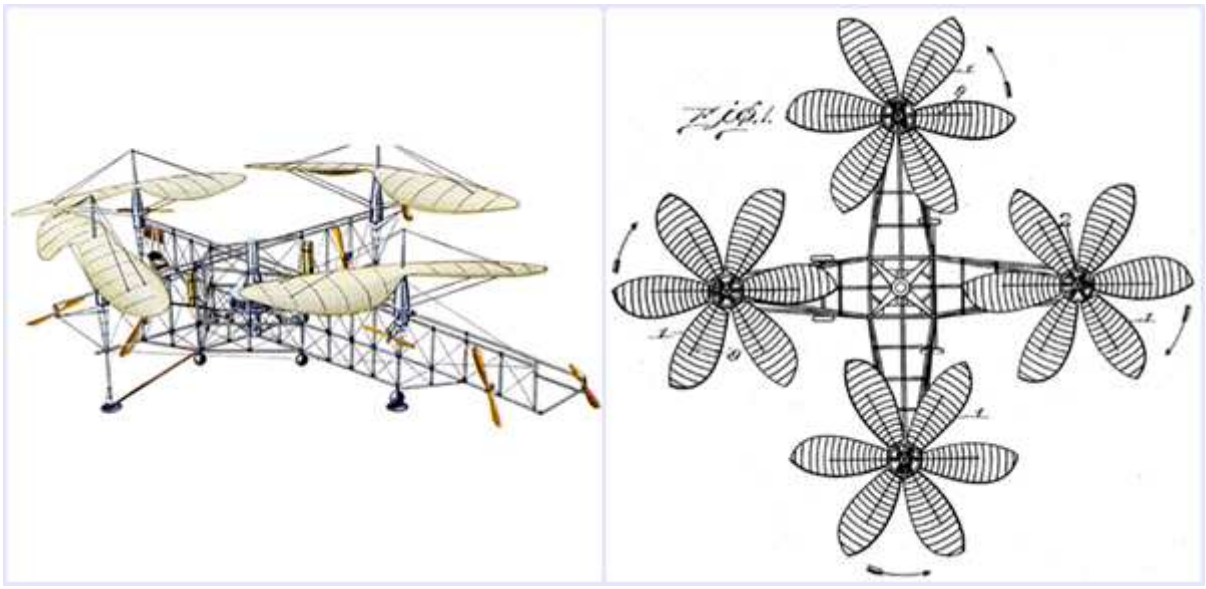

Figure 1.1 Drawing of the Oehmichen No. 2 (Left). Top view of De Bothezat helicopter 'Flying Octopus' as depicted in a US Patent in 1930 (Right).

Like other quadcopter designs of the time, the Octopus used additional horizontal rotors for pitch and yaw. It was reliable enough and a good proof of concept, performing those short flights at the time was bordering on the impossible, because mechanics was underdeveloped as a science. In fact this is something that we forget today, but there weren't any electronics to control anything. All the control workload was on the pilot, who used his mental agility with things like gears, shafts, and pulleys.

It was not until 1956 that the first practical quadcopter was flown. The Convertawings Model A was able to hover and manoeuvre with two engines. While previous attempts had kept the four lifting rotors spinning at the same speed and used additional rotors for control, the control of this helicopter was obtained by varying thrust between rotors which was less complicated. However this project was cancelled when the US military ceased their financial support.

In the 1950s, the US Army continued to develop several VTOLs. In 1957, the Army contracted with Curtiss-Wright Santa Barbara Division to build a 'flying jeep', the chief designer of the division was a former Nazi engineer and aircraft designer from Germany. The aircraft, named VZ-7, was of simple design, and the control system was also very simple, directional movement was controlled by varying the thrust of each individual propeller, with additional yaw control provided by moveable vanes fixed over the engine exhaust. The two prototype aircrafts were proved to be very easy to hover and manoeuvre. However, they were not able to meet the requirements specified in the Army's contract and the program was cancelled, also the intended job could be performed more easily and efficiently by conventional helicopters [1]. Since then, multicopters were nearly abandoned. During the following 30 years, there was not much improvement for this type of aircraft.

1.1.2 Growing period (1990-2005)

Until the 1990s, with the development of Micro-Electro-Mechanical System (MEMS), lightweight Inertial Measurement Unit (IMU) emerged. But the reduction of cost and size implied performance limitation and thus a more challenging control. Moreover, the miniaturization of inertial sensors imposed the use of MEMS technology, which was still much less accurate than the conventional sensors because of noise and drift, which made it difficult to directly use data. The research started to focus on how to eliminate the noise in the measurement of MEMS IMUs. Also, the computation speed of microcomputers had been improved significantly. This provided a possibility to design small multicopters which required a digital support to run their essential algorithms. At this phase, researchers at universities started to build models and design control algorithms for academic purposes [1].

Some pioneers started to build their own real multicopters and this novelty began to approach consumers via the RC toy market. During the early 1990s, a mini quadcopter was marketed in Japan and it may be the earliest generation of mini quadcopter, but it was designed for indoor use and offered about three minutes of flight time. There was also some other models in the US in 1999, and Germany in 2002. The basis for the further development of UAV quadcopters were advances in electronics and sensor technology, which were available on the market from around 2000 and appeared in series models from 2004 [1].

1.1.3 Development period (2005-2010)

Since 2005, researchers paid attention to multicopters, and some of them were not satisfied with simulation and started to build their own multicopters to test corresponding algorithms, especially attitude control algorithms. Although the algorithms were easy to design, it was not easy for a researcher to build a real multicopter, because E-commerce then was not mature and popular like it is today. The few multicopters designed were often not very reliable. Most of the time was spent on finding appropriate components, designing, and testing.

At that time, commercial multicopters were very expensive for mass customers, even without a camera. Moreover, they couldn't bear any useful payload and were not easy to control. After all, since smartphone devices had not been invented, they could be hardly used for entertainment purpose or taking pictures [1].

However, some sophisticated models for professional use were produced, like the MD4-200 from the German company Microdrones (figure 1.2). Launched in 2006, it was made predominantly of carbon fibre reinforced plastic and had a payload capability of 200g. Meanwhile, the French company Parrot initiated in 2004 a project named "AR. Drone", which was realised after 6 years of research and development. Tt was a successful ready-to-fly consumer drone and the first able to be controlled solely by a Wi-Fi connection.

Figure 1.2 Microdrone MD4-200, Professional quadcopter with + Configuration.

1.1.4 Activity period (2010-2013)

In this period more papers and conferences were made about drones. Many open source autopilots appeared which aided beginners in building multicopters, table 1.1 shows some major projects of open source autopilots and their websites. In this period also, smartphones with motion sensing and real-time video transmitting became popular, this have made control and use of drones easy and accessible.

Table 1.1 Some open-source autopilot projects.

Open source projects	Website
Ardupilot	http://ardupilot.org
Pixhawk	https://pixhawk.ethz.ch
Mikrokopter	http://www.mikrokopter.de
Parrot API (SDK)	https://projects.ardrone.org/embedded/ardrone-api/index.html
DJI DEVELOPER (SDK)	http://dev.dji.com/cn
Ehang GHOST (SDK)	http://dev.ehang.com
Taulabs	http://forum.taulabs.org

1.1.5 Booming period (2013-present)

At this stage, the research on multicopters tended to make them more autonomous and more cooperative[1]. This task can be carried out using various solutions based on visual cameras, Radio-Frequency ranging, LIDAR[2] and acoustic sensors. Visual cameras are extremely versatile sensors, being low-cost, lightweight and able to provide highly-accurate LOS estimates .They provide each UAV the capability to visually monitor the other members of the formation. However, this capability requires very complex algorithms to be fulfilled as well as satisfactory conditions of illumination [1] [3].

The increased academic interest for drones continued as well, in a search in the Scopus database (as for June 2019) using the keywords “drones” and “unmanned aerial vehicles” between 2009 and 2018. The research resulted in 2717 published journal papers, as shown in

[1] To fly in a coordinated manner, commonly known as swarms.
[2] Technique for determining the distance to an object by transmitting a laser beam, usually from an airplane, at the object and measuring the time the light takes to return to the transmitter (Encyclopædia Britannica).

Figure 1.3. There was an increasing trend, from 11 papers published in 2009 to 851 published in 2018. The ratio of drone-related papers to the total number of papers published per year in this database is shown in red, which also followed an ascending trend. This boost in research laid a solid foundation for the industry of drones [4].

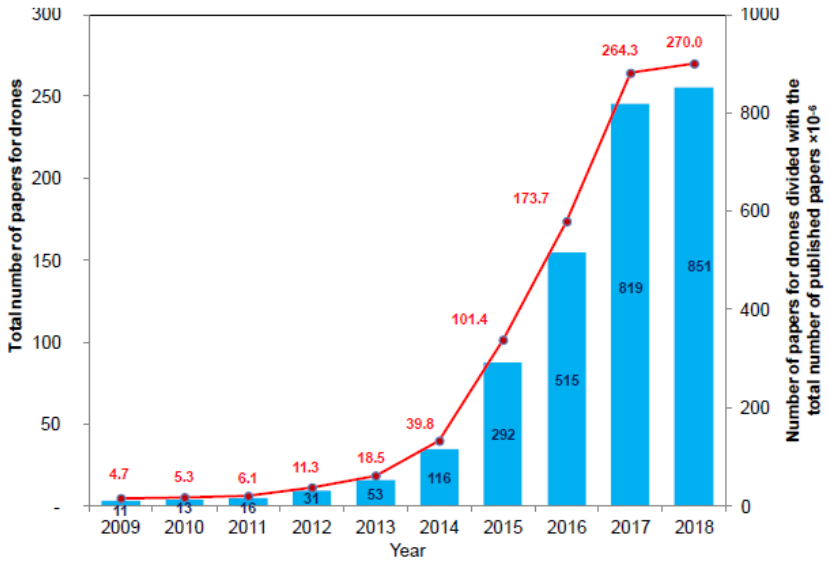

Figure 1.3 Evolution of papers published on drones from 2009 to 2018 **[4]**.

Modern multicopters are mostly of small scale, having an electric motor mated to each rotor. A flight computer constantly monitors the orientation of the helicopter and corrects for instability by changing not the pitch of the rotors but simply the rpm of the individual motors/rotors. This fixed pitch design is much simpler than the complex swashplate mechanics that are required for single rotor helicopters.

Presently, more and more multicopters are being designed and produced, the market has expanded in developed countries where operational legislations are more developed. This final period marked the domination of a Chinese company over the civil drones market, namely DJI, which made up a dominance of nearly 70% of the entire drone market in the world [5]. Table 1.2 lists a group of multicopters designed in this period.

Table 1.2 Notable quadcopter models of the last development period.

Model	Company	Launch year	Country
AR. Drone 2.0	Parrot	2013	France
AirDog	Helico Aerospace Industries	2014	Latvia
Splash Drone	Urban Drones	2015	USA
Mavic pro	Dji	2016	China
Wingsland S6	Wingsland Technology	2017	USA
UVify OOry	UVify	2018	USA
Dji Mavic Mini	Dji	2019	China

1.2 Classification of quadcopters

There are several classifications that have been developed by researchers and regulatory bodies to classify heavier than air UAVs. One classification [6] divides them into 3 classes according to the aircraft weight: micro air vehicles (less than 1kg), miniature air vehicles (less than 25kg) and heavier UAVs.

Drones can also be classified depending on the aerodynamic flight principle: fixed-wings UAVs and rotary-wings UAVs. Multicopters are part of the rotary-wings UAVs and are classified in tricopters, quadcopters, hexacopters, and octocopters. In terms of reliability, quadcopters have no possibility of landing if one motor fails, while a hexacopter can survive with limited yaw control and octocopters can fly and land with one motor failure [6].

Further to fixed-wings and rotary-wings aircraft, there is the flapping-wings category, which represents a novel subject of research. The last category is hybrid aircrafts which combine the characteristics of more than one category. Figures 1.4 and 1.5 in the next page illustrate these classifications.

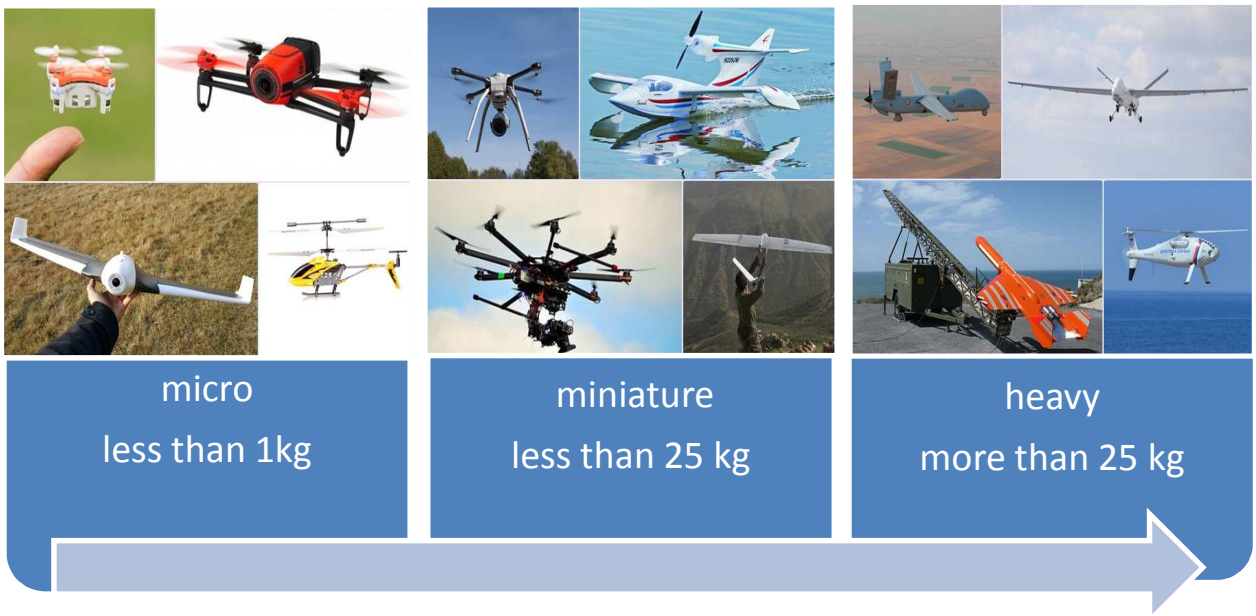

Figure 1.4 Classification according to weight [author].

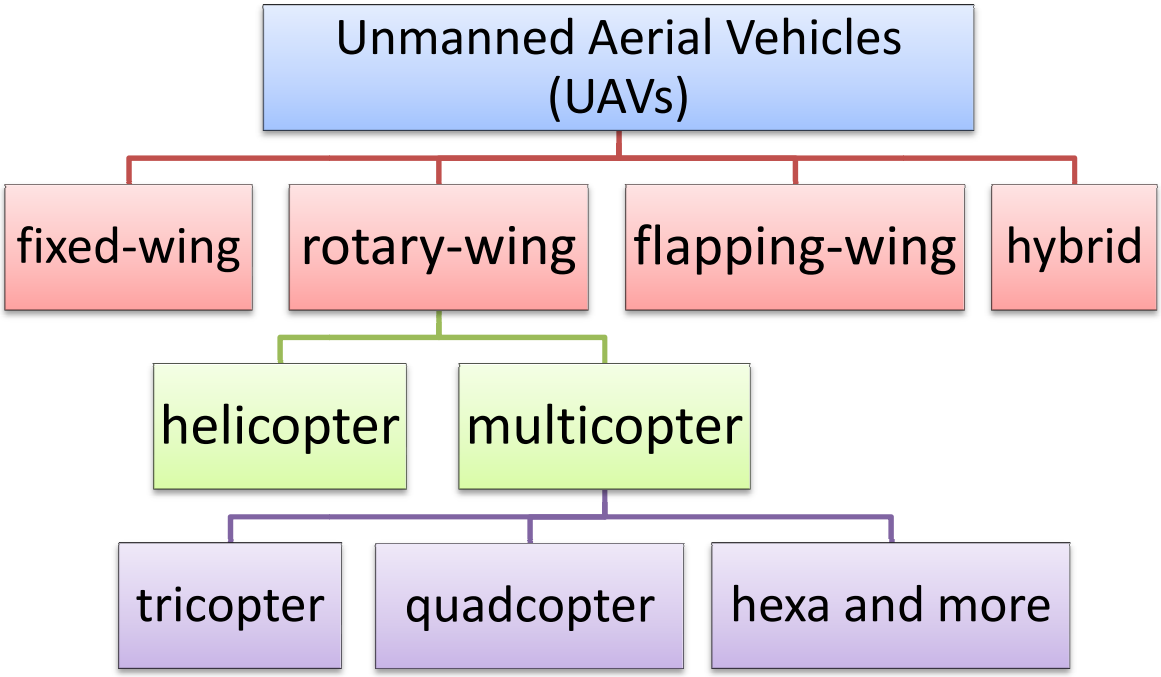

Figure 1.5 Classification according to aerodynamic flight principle [author].

1.3 Regulations and rules

Similarly to other aircrafts in general, quadrirotors and all other UAVs are subject to laws. Privacy and security issues that accompany these small aircrafts together with their fast integration into society, have made regulatory bodies introduce laws and rules around them. These rules vary between countries and may also vary between provinces of the same country.

As mentioned, drones might present a substantial risk to both safety and privacy. There is a very real risk of a drone colliding with an aircraft which can potentially cause fatalities if it collided with the windscreen of a plane. In 2018, about 90% of all Airprox[3] reports in the UK were suspected drone incursions. Also, there is public concern about drones being used to spy on homes, this technology can also present a new weaponry for terrorism [7].

If we look at the legislations of drones in three developed regions: Canada, USA and Europe, we can see that, while a case-by-case approach to authorisation was first adopted in the three regions, with special permission given for specific operations, all are now moving towards more a streamlined process whereby a properly certified operator (or licenced pilot) is authorised to conduct commercial operations, including complex operations with heavy vehicles beyond visual LOS, without making continual requests [8].

In Algeria, the situation of drones is comparatively more restricted: administrative bodies impose rigorous conditions to obtain a licence for operating a drone. It's difficult to get advantage from this technology especially for amateurs. In fact, to possess a drone requires a special certificate from many competent authorities, without which the drone is considered an illegal item. Therefore, customs and police frequently seize drones at airports and border crossings. Also, it is forbidden to fly near sensible zones, particularly security and administrative buildings [9] [10].

In an investigation of UAV regulations on the global scale, Claudia Stöcker et al. [11] divided the rules and measures around drones into three key aspects: 1) targeting the regulated use of airspace by UAVs; 2) imposing operational limitations; and 3) tackling the administrative procedures of flight permissions, pilot licenses and data collection

[3] An Airprox is defined as 'a situation in which, in the opinion of a pilot or air traffic services personnel, the distance between aircraft, as well as their relative positions and speed, have been such that the safety of the aircraft involved may have been compromised (Civil Aviation Authority of the UK).

authorization. We will simply name these aspects: 1) flight restriction zones and airspace use limitations, 2) operational limitations, and 3) registration and piloting requirements:

1.3.1 Flight restriction zones and airspace use limitations

There are areas where flying drones is prohibited, these areas are very similar worldwide and they include airports, military bases, critical infrastructures, diplomatic and consular representations, populated urban areas and natural parks (as showed in figure 1.6). Some manufacturers integrate geofencing systems on their drones, like DJI, which created no-fly-zones for its drones in 2013 and followed it by a more refined Geospatial Environment Online system, adding updates and new zones for prisons and nuclear power plants, while providing flexible self-unlocking for professionals. The following GEO 2.0 prevented the vehicle from accessing no-flight-zones around airports in 32 European countries. Drones using DJI software will have the safety zones integrated into their navigational systems and will be unable to breach the areas. This system will also impose temporary flight restrictions during major events or natural disasters, which will be based on data from regulatory body Eurocontrol [12].

Figure 1.6 Posted sign banning drones at a mountain trail, USA.

As UAVs pose a serious risk for manned aircrafts, they are usually not allowed to fly in controlled airspace and thus in the proximity of places where manned aircrafts land or take off, but a special authorization might be possible on a case-by-case basis [11]. Several countries have legislated a minimum distance away from airports, but some others have not determined a specific distance, requiring only a 'safety distance' [4]. The next diagram compares this distance for a group of countries.

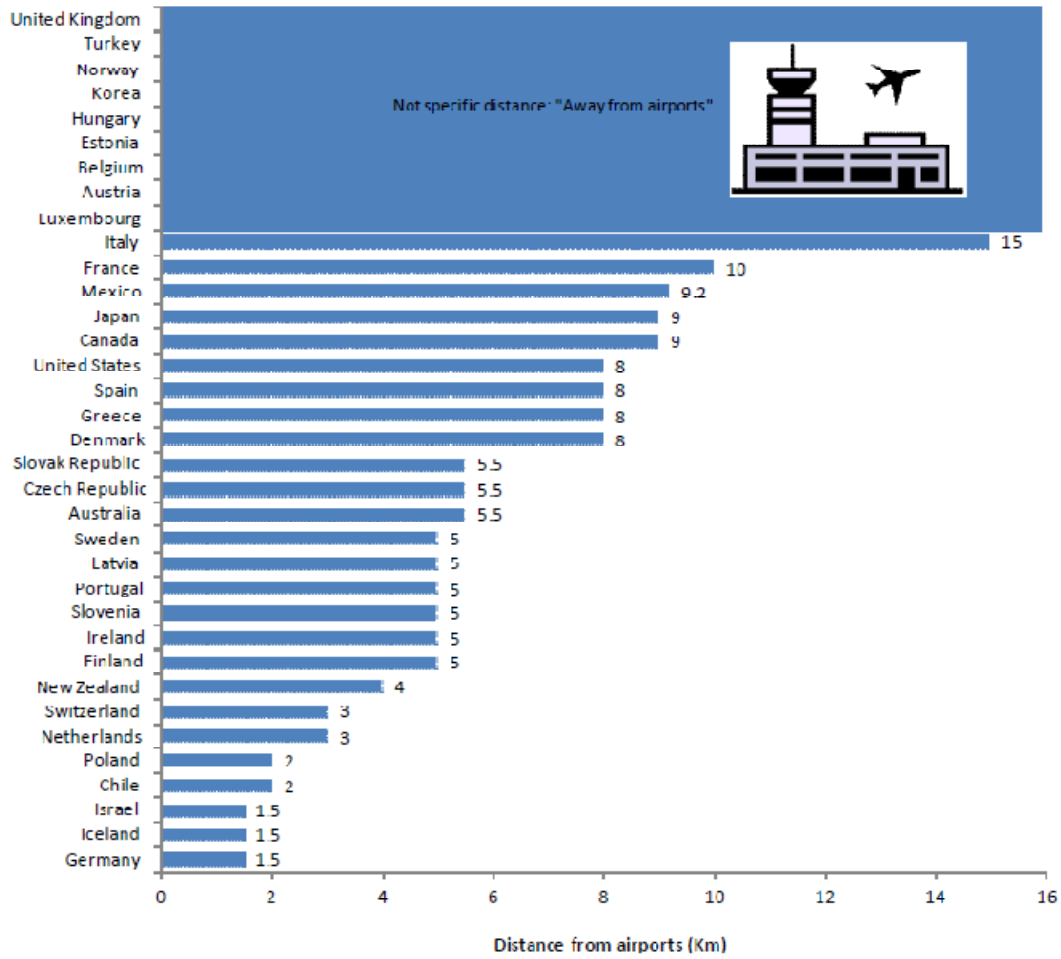

Figure 1.7 Limit distance for drone flights near airports for a group of countries **[4]**.

Drones must also stay away from emergency response efforts such as wildfires. In fact, a drone flies at the same altitude a firefighting aircraft flies (very low altitude, typically just a couple of hundred feet above the ground). This creates the potential for a mid-air collision or pilot distraction that could result in a serious or fatal accident. Unauthorized UAV flights could lead fire managers to suspend aerial wildfire suppression operations –by airtankers and helicopters- until the UAV has definitely left the airspace [13]. Figure 1.8 [from U.S. Forest Service] shows a warning poster on drone flying near wildfires.

Figure 1.8 Poster warning people not to fly drones near wildfires.

1.3.2 Operational limitations

The quadcopter must not go beyond a defined distance from its operator, whether it is an individual or a control vehicle. Maximum vertical distance (or altitude) varies widely from country to country, from 50m above ground to 150m above ground, This reduces the likelihood of a conflict with manned aircrafts. The other flight restriction is the horizontal distance from the operator which is typically regulated between 50 and 200m [4].

For the environment in which the drone operates. It is illegal to fly a drone directly over an individual or private property without consent. In the UK for example, drones must never be flown within 50 meters of vehicles, buildings, structures, and people, this can be interpreted as a total ban of drones in UK cities [7].

It is also essential for the normal user to keep the drone within visual LOS as depicted in figure 1.9, this means being able to see the aircraft directly with eyes (rather than through wireless video systems, binoculars or any other image enhancing devices) at all times.

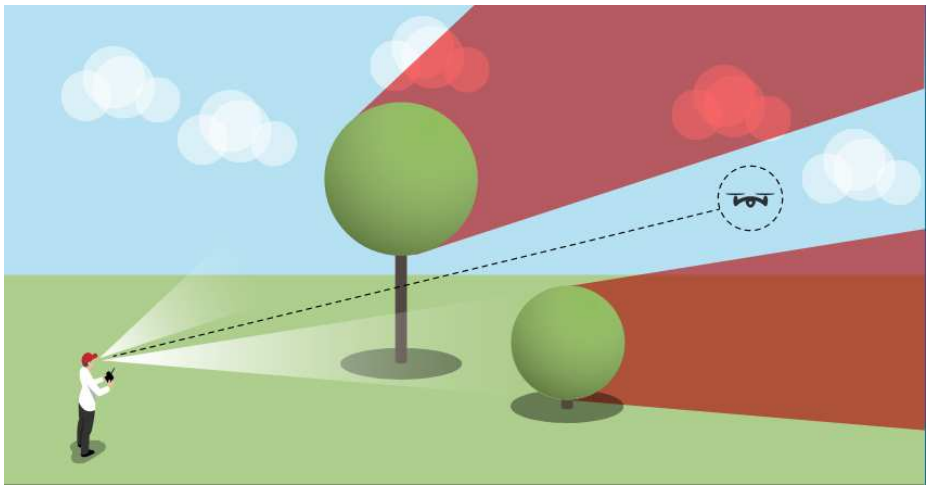

Figure 1.9 Normal operators are required to maintain direct eyesight of the drone [dronesafe.uk].

1.3.3 Registration and piloting requirements

Administrative procedures vary widely between countries: some countries do not envisage any application procedures for UAV operations below a certain MTOW—neither for the registration of the platform nor for a flight approval. For example, Drones less than 250g do not require a pilot licence or a registration in several countries like the US, the UK and Japan [7] [11]. In contrast, others follow a single-case flight authorization approach that entails a new application for each flight operation [11]. If the flight will be partly or entirely executed in controlled airspace, a notification to the air traffic control service with permission is obligatory in all cases.

Besides the UAV itself, there are conditions upon the UAV pilot. For recreational flights the operator must be over a certain age to prevent children from using this aircraft as a toy. Also, several legislations necessitate practical training, theoretical knowledge tests and medical tests.

1.4 Applications and uses

Quadricopters exist in various formats developed for different purposes. The advantages that this flying machines provide when combined with analytic tools have led to a new revolution which is manifested in many applications, we will cite the most useful ones for today's society:

1.4.1 In civil domain

UAVs were used commercially for the first time in Japan at the beginning of the 1980s. At that time, remote aircraft technology was expensive and cumbersome. Progress has surged forward in technological capabilities, regulations and investment support, providing many new possible applications [14]. Civil uses of quadcopters include:

1.4.1.1 Agriculture

UAVs can be a great solution for precision agriculture, they can offer a wide range of data, and with the right sensors they can collect crops information largely based on different bands of light reflected from the crops below. Different sensors collect different light bands, these sensors can be general RGB cameras to a specialised multi or hyperspectral sensor. The RGB sensor collects mainly the green light which specifies the amount of chlorophyll plants have, which is an indicator of photosynthesis. The near infrared (NIR) and red edge (RE) are reflected from healthy plants, NDVI[4] use NIR and RE light bands to distinguish areas where a crop is growing well from where not. A high NDVI signal means a healthy plant and a weak NDVI indicates problems or stressed plants. The NDVI maps enable targeted applications of treatments and therefore significant savings can be made using spot applications instead of full-field spraying [15].

Until recently, the most advanced form of monitoring used satellite imagery. The main limitation was that images had to be ordered in advance, could be taken only once a day and were not very precise as it can be seen in figure 1.10 .In addition, the services were extremely expensive and gave no guarantee of quality, which could easily drop on a cloudy day [14].

[4] NDVI (Normalized Difference Vegetation Index): graphical indicator used mainly in agriculture and forestry to differentiate plant from non-plant and healthy plants from plants under stress, initially used from satellites.

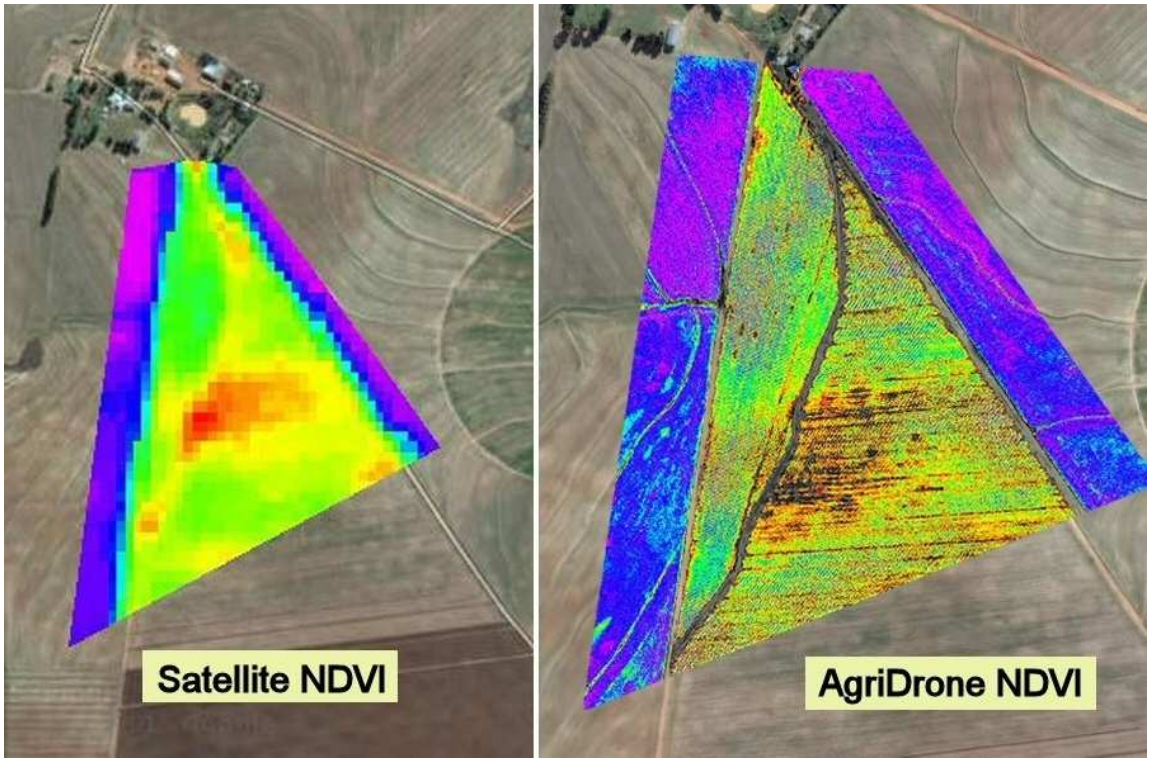

Figure 1.10 Resolution comparison between a satellite NDVI (left) and a drone NDVI (right), the two shots were for the same day [AgriDrone].

DronesDeploy -a company that builds software for drone mapping and solutions- describes the challenges of the early years of drones' employment in agriculture as being caused by two things: cost and usability. For all but a handful of major agronomist companies and farmers' cooperative, this was a very high price. For starters, user-friendly mapping solutions like DroneDeploy weren't yet on the market and a farmer had to possess a good deal of technical knowledge. Than the work had to be done locally, as opposed to in the cloud —requiring a powerful desktop pc— and it took upwards of two days which is -in urgencies time, such as spread of diseases- a long time. However, advances in technology have made the price of drone hardware far more accessible to the average agriculture professional [16].

The huge data sets available through rapid aerial surveys (only minutes for an average field) enable faster monitoring for crop health and progress, while farmers generally used to inspect the whole field on foot which took hours. Drones aircrafts can also be an effective solution for bird damage, they can deter aggressive birds who destroy and eat crops, by emitting sounds of a siren or of a natural predator.

1.4.1.2 Forestry

Globally, there are billions of hectares of natural forests used for wood production. The management of these lands can be very time-consuming and extremely tedious. With operations managers surveying such large lands over only a few days, and their conclusions can be inaccurate.

Satellite programs like Landsat are commonly used in forestry. However they are limited and not suitable for applications where very high spatial resolution is needed, such as individual trees or even leafs, or those requiring a very short period of satellite area revisiting. This is where drones come in, they generate highly accurate data (closer view) and can have multiple applications, this includes forest monitoring, mapping and territorial planning. In addition to obtaining images of very high spatial resolution, the superposition of images obtained with drones allows the derivation of height data, from a digital stereoscopy[5]. With this information on the height and the ground cover, the canopy height and the volume of the vegetation can be calculated (as showed in figure 1.11), and together with the land points, the necessary topographic information can be gathered [17].

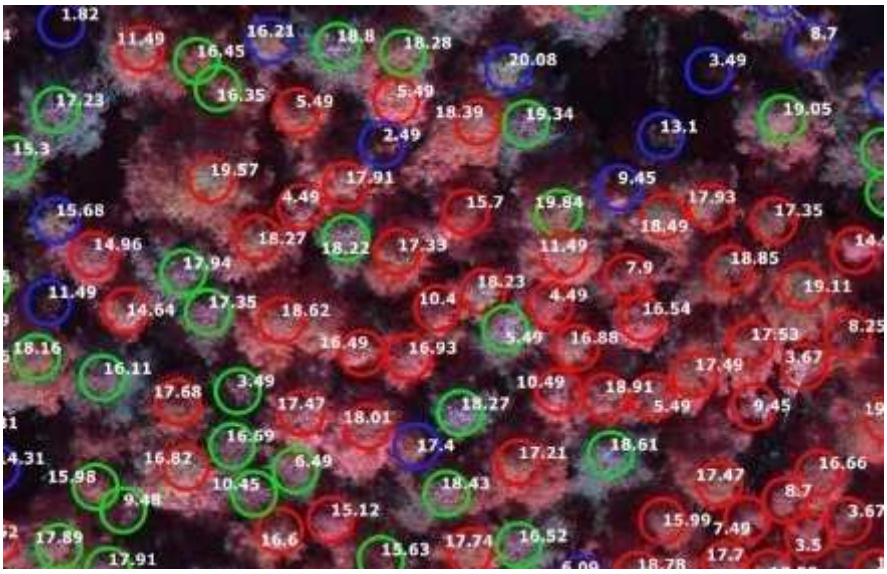

Figure 1.11 Drone imagery with digital post-treatment reveals individual trees locations and heights, each colour refers to a definite species [Mosaicmill Ltd].

[5] Stereoscopy, called commonly 3D, is a two-dimensional drawing or photograph that when viewed by both eyes appear to exist in three dimensions in space (Encyclopædia Britannica)

Drones can also collect real-time data of forest wildfires. Specifically, the simultaneous use of multiple drones, either autonomous or remotely controlled, allows larger areas to be measured and obtained complementary views of wildfires. Medium-and high-altitude drones are more suitable for flying over wildfire areas [18].

1.4.1.3 Search and rescue and disaster relief

Aerial Search and rescue (SAR) operations involving manned aircrafts are very costly. In addition, there is considerable risk in using manned aircraft for certain SAR operations, and situations in which manned aircraft are constrained are common (e.g., fog, inconvenient weather). In many situations Drones are a better alternative, they have proven very useful in disaster relief operations and humanitarian aid distribution, they have been recently used as a tool to support several aspects of disaster response, such as gathering information on the ground state, 3D mapping, situational awareness, logistics planning and damage assessment. They have also been used to support SAR missions through delivery of live-saving equipment such as life vests (see figure 1.12), or allowing for audible communication through speakers with people once they are located.

Figure 1.12 Drone delivery of a life vest (in red) for two stranded individuals in a river, USA.

Innovations in camera technology have had significant impacts on the growing use of drones. UAVs outfitted with thermal imaging cameras have provided emergency response teams with an ideal solution for identifying victims who are difficult to spot with the naked eye. According to Claire Burke et al. in [19], automated detection algorithm in drones were

effective in searching humans using TIR[6] imagery, they found the volunteers in almost all scenarios. False positives for the automated detection were warm vehicle engines, warm building roofs and reflective/warmed rocks. These were easily excluded as not humans by visual inspection. Figure 1.13 (from the same source) shows a comparison between TIR and RGB data taken from a drone.

Figure 1.13 RGB (left) and TIR (right) images taken from the drone showing the same scene for a search and rescue scenario. The volunteer hiding in rocks is very difficult to discern in the RGB image but appears as a bright source in the TIR image **[19]**.

While there is a huge potential in the use of drones for SAR operations, it must be noted that they cannot do everything. They are relatively ineffective when compared to rescue teams: drone flights could not help or directly rescue people – they can only aid them and bring supplies. A camera eye-in-the-sky is only of practical use in saving lives if a drone operator knows what they are looking for. A drone camera has a relatively narrow field of view compared to a human observer in a helicopter who could scan a wider area [20].

1.4.1.4 Logistics and transport Systems

Quadcopters could provide major agility in first-and last-mile networks: i.e. the first and last short segments of delivery and not in the main segment. The concepts of sending packages to a client's doorstep have already gained attention and Amazon is running Amazon Prime Air, which seeks to automate last-mile delivery of packages using small drones [14]. In May 2019, DHL Express with Ehang have launched a fully automated and intelligent drone delivery solution to tackle the last-mile delivery challenges in the urban areas of China.

[6] Thermal InfraRed (TIR) is an imaging technique that displays heat which is radiated from relatively hot objects, commonly used in an aerial platform to find objects that are difficult to see using optical techniques for various reasons. (www.imageair.com.au/thermal-infrared-tir)

While having a parcel automatically delivered by a drone may seem like an obvious commercial application, it's far from straightforward. In addition to regulatory restrictions and technical immaturity (short drone battery life, limited payload), there are other challenges. Given cities' urban density, people ordering goods online are situated within a relatively small territory; using drones to deliver parcels could see an airspace filled with drones that risk crashing into one another [14]. Also, drones were proved to be economically inefficient compared to ground solutions such as truck deliveries. Unless for missions involving high value and time-sensitive deliveries, using drones for regular parcel delivery is therefore unlikely to be feasible.

1.4.1.5 Infrastructure

In construction industry, controlling infrastructures might contain hazardous tasks for human worker or tasks that cannot be accomplished without special and expensive equipments. In those tasks drones are an ideal replacement. Not only can they perform unsafe work, but they also make it easier to acquire various data sets. For instance, some supplies that require quantitive assessment cannot be measured by the human eye (e.g. piles of sand). The volume of such assets can easily be gauged using drones, making inventory assessments faster, more cost-efficient and much more accurate.

Drones have various applications in project management in every stage of the project: they can carry out an initial research about the terrain and its topography. During the construction phase, drones can measure progress or change by comparing current state to a baseline measurement already taken. Drones facilitate quick and accurate checks as input for progress reports. Discrepancies between the current state and initial theoretic plans can be seen in detail, enabling construction works to be followed up and documented [14].

1.4.1.6 Entrainment and Media

One of the most popular fields for drone-powered solutions is the media and entertainment industry, they have wide application in the advertising industry, aerial photography and filming.

Action sequences and dramatic panoramas using drones offer numerous advantages over traditional methods of capturing aerial imagery such as helicopters, which can't get too

close to the subject due to its size and the large amount of noise and wind it generate. Drones are also very advantageous from cost perspective. However, although drones can be extremely cost effective for certain applications, when it comes to aerial views, they haven't fully vanquished the use of helicopters. Their limited battery life still makes some uses impractical, and they can be flown legally only at relatively low altitudes.

1.4.2 In non-civil domain

Non-civil applications of drones include military applications and law enforcement. As the majority of drone technologies could have dual-use (civil and military) characteristics, it is not uncommon for the military to acquire civilian-developed technologies and adapt them to suit military tasks and requirements.

1.4.2.1 Military applications

Drones have become known for launching military attacks from great distance, which is reported to be used in a cold-blooded way by some developed countries. However, these drones are fixed-wing UAVs – not quadcopters -. Quadcopters are only capable of carrying small and lightweight explosive devices. In addition to payload limits, quadcopters aren't able to fly for longue periods (due to short battery life). Military quadcopters role in war zones is mainly reconnaissance of unknown areas/buildings, enemy tracking, and, real time and near real time surveillance.

Although the apparent similarity in form and components, military quadcopters are far more costly than recreational drones. Several military drones are autonomous to a certain degree and are equipped with advanced surveillance and communication devices.

1.4.2.2 Law enforcement and surveillance

Security departments (police for example) are already making use of drones to help them on different mission types: They help investigating suspects that are believed to be armed and dangerous while maintaining a safe distance which gives officers real-time information to assess the threat, they also offer the opportunity to conduct surveillance operation without being spotted. Another use is crowd monitoring, for example in large gatherings and protests, which allows the police to track any suspect through the crowed.

Surveillance is one of the multiple tasks that drones are tasked to do in high risk scenarios. The UAVs can be used to collect data beyond the range of fixed sensors. Moreover, the management of traffic incidents can also be improved drastically with the help of such technology. However, despite of a number of advantages, UAVs still have some significant limitations that need to be addressed. The technical limitations i.e. limited battery time, weather constraints along with the safety and privacy concerns are the biggest hindrances in making this technology more effective. Therefore, the current low cost technology can be utilized most effectively by combining it with the other traffic data collection apparatus. With the passage of time, the UAV technology is rapidly being accepted as a very useful and dynamic technology, particularly for the collection of detailed and accurate visual data [21].

1.5 Notable recent models

1.5.1 DJI Mavic series

The Mavic is a series of compact quadcopter drones for personal and commercial aerial photography, released by the Chinese company DJI. 6 models of Mavic have been realised, the first one was the Mavic pro (shown in figure 1.14), launched in 2016. The Mavic pro is foldable and weighs 743 g. The drone is capable of capturing 4K video, having a flight range of 6.9 km and a flight time of 27 minutes. The Mavic can sense obstacles up to 15m away and bypass them or brake to hover, which reduce accidents.

Figure 1.14 Mavic Pro, the first model in the DJI Mavic

In 2019, DJI announced the Mavic Mini, also designed mainly for photography. It shares similar design characteristics with the Mavic Pro, though notable for its portability and overall small size (see figure 1.15). DJI's marketing behind the Mavic Mini focuses on the weight of the drone at 249 grams, allowing it to bypass drone registration regulations in several western countries without having to register it with the government. Being only 1g short, this drone is not subject the more stringent requirements on drones that weight 250 grams and up.

Figure 1.15 Illustration of the compact package of the DJI Mavic Mini.

1.5.2 Parrot AR.Drone series

The AR.Drone was a successful recreational quadcopters, launched in 2010 by the French company Parrot. The technology of AR. Drone was very advanced at the time, it was the first commercial product to adopt the optical flow method in velocity estimation of multicopters: it used a downward-looking camera to measure optical flow and two ultrasonic range finders to measure the altitude. Based on this, its velocity could be obtained by using estimation algorithms. Furthermore, it offered a Software Development Kit (SDK) so that researchers could develop their own applications which meant it was equipped with research potentials. As a result, the product spread rapidly in academia [1].

Technically, the onboard computer runs a Linux operating system, and communicates with the pilot through a self-generated Wi-Fi hotspot. It provided an average of 12 minutes of flight time and the control was achieved by a smartphone or tablet device and has no controller to come with it.

Two years later, the AR.Drone 2.0 was realised. In the same way, it was designed to be controlled by mobile operating systems. The Parrot 2.0 could, besides taking photos, record videos in 720p HD and directly sends the footage to a connected HD device. The flying time remained the same, but in that time it was the standard time.

Two interchangeable hulls were supplied with the drone: an indoor body with foam rings surrounding the rotors to protect the propellers (see figure 1.16), and an outdoor body that allowed for increased maneuverability.

Figure 1.16 Parrot AR. Drone 2.0 equipped with its protective indoor hull.

1.5.3 Donecle Drone

Donecle is a Toulouse-based aircraft manufacturer which develops autonomous inspection UAVs. The company offers single UAVs and swarms of UAVs to visually inspect the exterior of airliners. Autonomous navigation of the UAVs is based on laser positioning technology. During the flight, cameras mounted on the UAVs photograph the exterior surface of the aircraft. Algorithms analyse the images and provide a diagnostic report about the aircraft surface. A human operator chooses a flight plan for the required inspection and a qualified inspector then validates the reports.

Figure 1.17 Donecle drone inspecting autonomously an AirFrance aircraft.

The drone flies autonomously on a preplanned flight and takes 1,500-1,900 pictures per narrow body aircraft. This solution will contribute to a paperless process and to better traceability of inspections. While the drone system identifies more abnormalities, about 10-20% of which are false positives, airliners says there is still an advantage over people and equipment moving around the aircraft [22].

1.5.4 Airbus Skyways drone

In March 2019, Airbus has begun shore-to-ship trials in Singapore with its Skyways parcel delivery drone (figure 1.18, from Airbus). This marks the first time drone technology has been deployed in real port conditions to deliver a variety of small, time-critical maritime essentials to working vessels at anchorage.

Figure 1.18 Airbus Skyways delivery drone.

The trials are being undertaken in conjunction with a maritime logistics and port services company. During the trials, Skyways octacopter drone will lift off from the pier with a payload capability of up to 4 kg, and navigate autonomously along pre-determined 'aerial corridors' to vessels as far as 3 km from the coast. Skyways is planned to be commencing another trial phase delivering air parcels autonomously in an urban environment, at the National University of Singapore [23].

1.5.5 Ehang 184

Ehang 184 is a large passenger drone built by the Chinese company Ehang. By 2018, 30 to 40 single pilot EHang 184 have been built but the aircraft is still under tests. It has a net weight of 200kg, and can carry a load of up to 100kg for 23 minutes of duration at sea level.

The EHang 184 is constructed using composite material with carbon fibre and epoxy, and aerial aluminium alloy. It is embedded with a fail safe system that will make the aircraft land in the nearest possible area to ensure safety in the event of malfunction or disconnect of components. The 184 autonomous aerial vehicle is powered by eight superimposed electric motors (figure 1.19, from Ehang), which generate maximum output power of 106KW and allow to reach a speed 100 km/h.

The aircraft features an automatic navigation system which doesn't require a professional pilot. The first operational network of these air taxis will be in Guangzhou in China. The benefits of such a network will be especially valuable for cities like Guangzhou, where rapid growth has led to plenty of traffic and high density at the ground level.

Figure 1.19 Ehang 184, autonomous manned quadcopter for air transport uses.

2 Basics and Dynamics of Quadcopters

Chapter 2 Introduction

The goal of this chapter is to establish the equations of movement for the quadcopter in both displacement and angular rotation, six differential equations will be needed to describe completely the motion of the vehicle.

But we will first introduce the aircraft and its different configurations, then we will describe the movements it can execute, then the associated frames of reference and the attitude representation methods, which are: the famous Euler Angles method, Direction Cosines and quaternions. Once the reference frames and their relating relations have been defined, we will derive the equations of motion for the six-degree-of-freedom model.

How to model the real quadcopter, with its diverse movements and states, in a mathematical model?

2.1 Description of a quadcopter

Multicopter systems are generally composed of several simple components such as the airframe, propulsion system, command and control system. On the other hand these compositions are complex in the intricate way that components connect and constrain with each others.

The quadrirotor cannot generate any wing lift. Instead it depends solely on thrust forces created by the motors to lift itself and to navigate as well. The other forces that affect the quadcopter are drag and weight, these forces generate their respective moments around the centre of gravity (CG).

To ensures that the net torque generated by every propeller around the CG of the quadcopter is zero, the direction of propellers rotations are alternated, i.e. clockwise (CW) and then counterclockwise (CCW), as represented in the figure 2.1. The aircraft wouldn't be stable and navigable if all the motors rotated in the same direction and a strong yaw rotation would result.

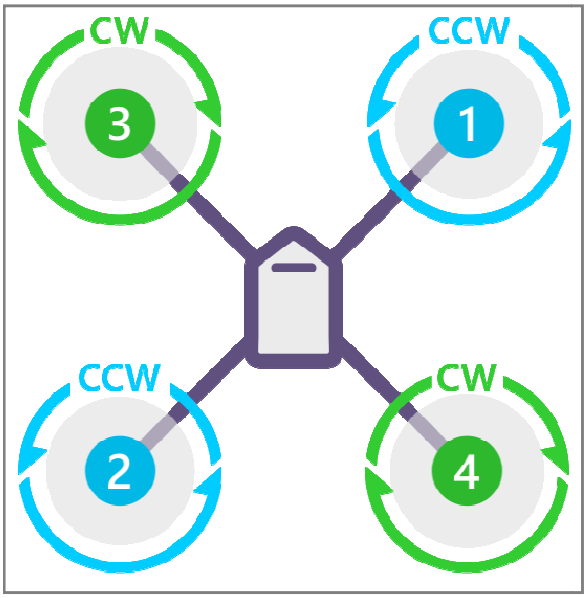

Figure 2.1 Rotation directions of the quadcopter propellers.

2.2 Airframe configurations

The basic quadcopter is a centre platform from which four beams are extended, motors are attached at the end of each beam. The common propulsion configuration is of a motor spinning a propeller. Propellers can be of a tractor type and motors are placed on top, or less commonly, of a pusher type and motors are placed at the bottom (figure 2.2).

Another propulsion form is the co-axial form, where two propellers are positioned one above the other and are driven by two separate motors, the upper propellers work as tractors, while the lower units are pushers (figure 2.2).

Figure 2.2 Propulsion configurations: tractor (top left), pusher (top right), and co-axial (bottom).

The advantage of the co-axis form is increased payload capacity (due to the increased number of propellers) with the same volume of platform kept. However, there is an interference between the flows of the two propellers resulting in a total thrust that is lower than two isolated propellers: the two propellers of the co-axis form are approximately equivalent to 1.6 propellers as the common form [1].

As for the airframe, there are 3 main configurations: X configuration, + configuration (called plus or cross) and H configuration, the motors always alternate in rotation direction, see figure 2.3.

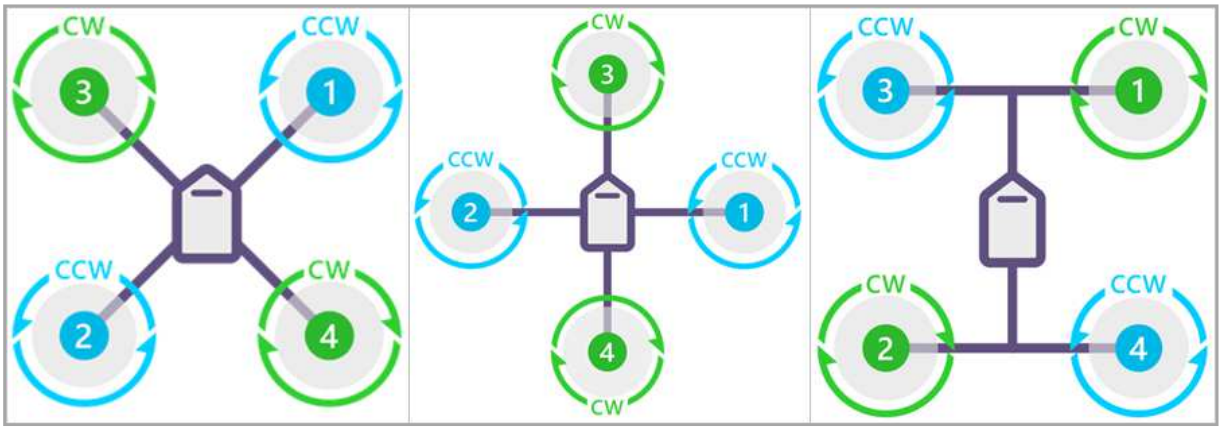

Figure 2.3 Fuselage configurations from left to right: X configuration, + configuration, and H configuration.

The forward direction is centred between two beams for the X configuration, and is aligned with a beam for the plus configuration.

Compared with plus-configuration quadcopters, the popular X-configuration quadcopters have higher manoeuvrability because more rotors are involved in pitch and roll control, and less occlusion of the forward field of view [1] which is an advantage for research and photography objectives. In addition, this configuration is more responsive while correcting induced external perturbations [24].

2.3 Control and movements of a quadricopter

The control of quadrotor involves attitude control (orientation) and position control (displacement), similar to fixed-wings aircrafts. The main difference is that, due to the unique body structure as well as rotor aerodynamic , the attitude dynamics and position dynamics are strongly coupled [25].

The motion of the quadrotor is controlled by varying the rotation speed of the four rotors to change the thrust and the torque produced by each one, the possible movements are:

- Pitch movement, obtained by increasing (respectively reducing) the speed of the rear motor –or motors– while reducing (respectively increasing) the speed of the front motor, which results also in a backwards (forwards) translation movement.
- Roll movement, obtained in the same way using the lateral motors and it produce a sideward translation movement.

- Yaw movement, obtained by increasing (decreasing) the speed of two aligned motors while decreasing (increasing) the speed of the other motors.
- Vertical movement, obtained by varying equally the speed for the four motors.

We can see that the quadcopter has 6 DOF but with only 4 control forces , the system is then underactuated.

2.4 Coordinate frames of reference

Before discussing the modelling of the quadrotor and the derivation of the aircraft equations of motion. We start with the definition of reference frames or coordinate systems. To describe the motion of a general aircraft moving in the air, two major reference frames are used in aeronautics [26]: the Earth reference frame and the aircraft body reference frame.

2.4.1 Earth frame

The Earth (or inertial) frame F_e ($o_e x_e y_e z_e$) is used to study the aircraft's dynamic states relative to the ground and to determine its three-dimensional position. The earth frame is assumed to be inertial with a flat $x_e y_e$ plane. The origin o_e can be chosen arbitrarily at a fixed point on the surface or the centre of the Earth [1]. The $o_e x_e$ axis points to a certain direction in the horizontal plane, and the $o_e z_e$ axis points perpendicularly to the ground (or upwards, in other references). Lastly, the $o_e y_e$ axis is determined according to the right-hand rule.

If we set the x axis to point to the north, the y axis to point to the east and the z axis down, then this frame is commonly referred to as the local North-East-Down frame (NED frame). The Earth frame is a convenient frame to express aircraft translational and rotational kinematics. Additionally, one force acting on the aircraft, weight $\boldsymbol{w}$, remains fixed in the z_e direction (see figure 2.4). The position vector $\boldsymbol{\xi} = (x\ y\ z)^{\mathrm{T}}$ and attitude angles of the system are defined in this reference frame.

2.4.2 Body frame

The body frame F_b ($o_b x_b y_b z_b$) is attached to the aircraft and has the origin o_b set as the centre of mass. The $o_b x_b$ axis points to the forwards direction in the symmetric plane of the aircraft. The $o_b z_b$ axis points downwards or upwards, in the symmetric plane of the aircraft. The $o_b y_b$ axis is determined according to the right-hand rule.

The body frame is often of interest because the origin and the axes remain fixed relative to the aircraft. This means that the relative orientation of the Earth and body frames describes the aircraft attitude. Also, the direction of the force of thrust is fixed in the body frame and is pointing in the z_b direction (see figure 2.4).

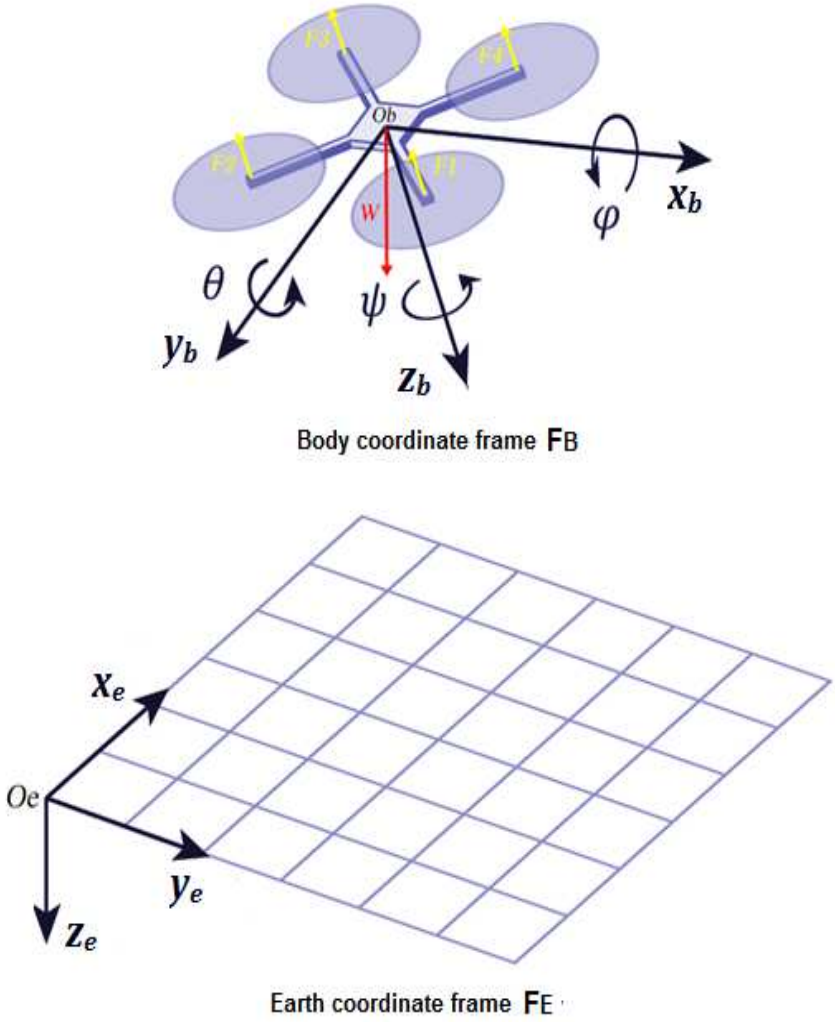

Figure 2.4 Body frame and Earth frame.

2.5 Transfer between the frames of reference

After defining the reference frames, we will define the relation between them, the relative attitude between these frames is a combination of:

- a linear translation of the origin from the Earth frame, by a distance $\boldsymbol{\xi} = [x \quad y \quad z]^{\mathrm{T}}$, And,
- an angular rotation which describes the orientation of the body with respect to the Earth.

The translation is handled quite easily by specifying the position vector $\boldsymbol{\xi}$ from o_e to o_b. It's rotations that are more complicated and more important in attitude control.

To express a vector in the coordinate system of a rotated frame relative to an original frame, we can use a multitude of methods: Euler angles, direction cosines and quaternions.

2.5.1 Euler angles

The Euler angles are three successive orthogonal rotations that express one arbitrary rotation between two reference frames. Various possible combinations exist and their order is important, in aerospace there is a convention which is called the ZYX convention. The ZYX sequence yields the following transformation matrix $\boldsymbol{R}_e^b$, which transforms from the Earth frame to the body frame:

$$\boldsymbol{R}_e^b = \begin{bmatrix} \mathrm{c}\,\theta\,\mathrm{c}\,\psi & \mathrm{c}\,\theta\,\mathrm{s}\,\psi & -\mathrm{s}\,\theta \\ -\mathrm{c}\,\phi\,\mathrm{s}\,\psi + \mathrm{s}\,\phi\,\mathrm{s}\,\theta\,\mathrm{c}\,\psi & \mathrm{c}\,\phi\,\mathrm{c}\,\psi + \mathrm{s}\,\phi\,\mathrm{s}\,\theta\,\mathrm{s}\,\psi & \mathrm{s}\,\phi\,\mathrm{c}\,\theta \\ \mathrm{s}\,\phi\,\mathrm{s}\,\psi + \mathrm{c}\,\phi\,\mathrm{s}\,\theta\,\mathrm{c}\,\psi & -\mathrm{s}\,\phi\,\mathrm{c}\,\psi + \mathrm{c}\,\phi\,\mathrm{s}\,\theta\,\mathrm{s}\,\psi & \mathrm{c}\,\phi\,\mathrm{c}\,\theta \end{bmatrix} \tag{2.1}$$

Where c and s denote cos and sin respectively. The derivation of the rotation matrix (2.1) is shown in details in Appendix A.1.

To perform the inverse transformation we multiply by $\boldsymbol{R}_b^e$, which is the inverse of the previous transformation matrix:

$$\boldsymbol{R}_b^e = \boldsymbol{R}_e^{b\,-1}$$

$$\boldsymbol{R}_b^e = \begin{bmatrix} \mathrm{c}\,\theta\,\mathrm{c}\,\psi & -\mathrm{c}\,\phi\,\mathrm{s}\,\psi + \mathrm{s}\,\phi\,\mathrm{s}\,\theta\,\mathrm{c}\,\psi & \mathrm{s}\,\phi\,\mathrm{s}\,\psi + \mathrm{c}\,\phi\,\mathrm{s}\,\theta\,\mathrm{c}\,\psi \\ \mathrm{c}\,\theta\,\mathrm{s}\,\psi & \mathrm{c}\,\phi\,\mathrm{c}\,\psi + \mathrm{s}\,\phi\,\mathrm{s}\,\theta\,\mathrm{s}\,\psi & -\mathrm{s}\,\phi\,\mathrm{c}\,\psi + \mathrm{c}\,\phi\,\mathrm{s}\,\theta\,\mathrm{s}\,\psi \\ -\mathrm{s}\,\theta & \mathrm{s}\,\phi\,\mathrm{c}\,\theta & \mathrm{c}\,\phi\,\mathrm{c}\,\theta \end{bmatrix} \tag{2.2}$$

We note that $\boldsymbol{R}$ is an orthogonal matrix, that means that its inverse equals its transpose, in other words it is sufficient to turn rows into columns to get the matrix of the inverse transformation.

For this technique, there is a singularity that shows up at pitch angles ±90 degrees (the aircraft pointing straight up or straight down), and the numerical calculations won't be able to determine the right orientation of the aircraft, this phenomenon is called the gimbal lock.

To acquire information about the angular velocity of the quadrotor, IMUs or gyroscopes mounted on board of the aircraft measure angular rates (or angular velocities) which are converted to Euler angular rates by another transformation matrix $\boldsymbol{D}$.

$$\boldsymbol{D}(\psi, \theta, \phi) = \begin{bmatrix} 0 & \sin\phi/\cos\theta & \cos\phi/\cos\theta \\ 0 & \cos\phi & -\sin\phi \\ 1 & sin\phi\tan\theta & \cos\phi\tan\theta \end{bmatrix} \tag{2.3}$$

Note that this transformation matrix, unlike $\boldsymbol{R}$, is not orthogonal

The Euler Angle rates can be then computed as:

$$\dot{\boldsymbol{\eta}} = \boldsymbol{D}\,\boldsymbol{\Omega} \tag{2.4}$$

where

$$\dot{\boldsymbol{\eta}} = \left[\dot{\phi}\ \dot{\theta}\ \dot{\psi}\right]^{\mathrm{T}}$$

and

$$\boldsymbol{\Omega} = [p\ q\ r]^{\mathrm{T}}$$

Appendix A.2 gives a detailed explanation on the Euler rates, the aircraft angular rates and the relation between the two.

2.5.2 Direction cosines matrix

An alternative method is the Direction Cosines Matrix (DCM) method, also called rotation matrix method [27]. Let $\boldsymbol{v}$ be a vector with the components

$$\boldsymbol{v}_{\mathrm{a}} = \begin{bmatrix} v_{a1} \\ v_{a2} \\ v_{a3} \end{bmatrix} \text{ in } \mathrm{F_a}$$

and

$$\boldsymbol{v}_{\mathrm{b}} = \begin{bmatrix} v_{b1} \\ v_{b2} \\ v_{b3} \end{bmatrix} \text{ in } \mathrm{F_b}$$

The component of v_{a1} in the direction of x_{bi} is $v_{a1} \cos\theta_{i1}$ where θ_{i1} denotes the angle between $o_b x_{bi}$ and $o_b x_{bi}$. Thus by adding the three components of v_{aj} in the direction of x_{bi} we obtain

$v_{bi} = \sum_{j=1}^{3} l_{ij}\, v_{aj} \quad i = 1 \ldots 3$

$l_{ij} = \cos\theta_{ij}$ Are the nine direction cosines, we write the sum equation in terms of matrices:

$$\boldsymbol{L}_a^b = \left[l_{ij}\right] = \begin{bmatrix} cos\theta_{11} & cos\theta_{21} & cos\theta_{31} \\ cos\theta_{12} & cos\theta_{22} & cos\theta_{32} \\ cos\theta_{13} & cos\theta_{23} & cos\theta_{33} \end{bmatrix} \tag{2.5}$$

And the transformation from reference frame *a* to reference frame *b* is:

$$\boldsymbol{v}_b = [\boldsymbol{L}]_a^b\, \boldsymbol{v}_a$$

2.5.3 Quaternions

Quaternion algebra was introduced by in 1843, but neither of its theorems could be applied in real systems due to the limited computational resources at that time [1], the first published report bringing quaternions to the attention of airplane flight simulation engineers was in 1957 [28].

A quaternion can be seen as a four-elements vector, composed of one real element and three complex elements. We adopt here the following representation:

$$\boldsymbol{q} \triangleq \begin{bmatrix} q_0 \\ q_1 \\ q_2 \\ q_3 \end{bmatrix} \triangleq \begin{bmatrix} q_0 \\ \boldsymbol{q}_\mathbf{v} \end{bmatrix} \tag{2.6}$$

where $q_0 \in \mathbb{R}$ is the scalar part of $\boldsymbol{q}$, and:

$$\boldsymbol{q}_\mathbf{v} = \begin{bmatrix} q1 \\ q2 \\ q3 \end{bmatrix} \in \mathbb{R}^3 \tag{2.7}$$

$\boldsymbol{q}_\mathbf{v}$ is the vector part (subscript v for vector). For a scalar $s \in \mathbb{R}$, the corresponding quaternion is defined as:

$$\boldsymbol{q} = \begin{bmatrix} s \\ \mathbf{0}_{1\times3} \end{bmatrix} \tag{2.8}$$

For a vector $\boldsymbol{v} \in \mathbb{R}^3$, the corresponding quaternion is:

$$\boldsymbol{q} = \begin{bmatrix} 0 \\ \boldsymbol{v} \end{bmatrix} = \begin{bmatrix} 0 \\ v_x \\ v_y \\ v_z \end{bmatrix} \tag{2.9}$$

Quaternions have their own operation rules (addition, multiplication...) which are used to formulate the frame rotation. In this thesis, we will take directly the final results, details about the theory of quaternions may be found in more expanded works like [1] and [27].

The rotation from an original frame a to a rotated one b can be represented by a quaternion. Specifically, if θ is the angle of rotation and the vector $\boldsymbol{u} = \begin{bmatrix} u_x & u_y & u_z \end{bmatrix}^\mathrm{T}$ is a unit vector representing the axis of rotation, then the elements of the transformation quaternion are defined as:

$$\boldsymbol{q}_a^b = \begin{bmatrix} q_0 \\ q_1 \\ q_2 \\ q_3 \end{bmatrix} = \begin{bmatrix} \cos\dfrac{\theta}{2} \\ \boldsymbol{u}\sin\dfrac{\theta}{2} \end{bmatrix} \tag{2.10}$$

Instead of performing three successive rotations on an orthogonal frame like the Euler angles require, the quaternion represents orientation by achieving a single rotation around a unique axis $\boldsymbol{u}$ (the quaternion vector) by an angle of θ. The rotation of a vector $\boldsymbol{v}$ is given by the operation:

$$\boldsymbol{v}_\mathbf{b} = \boldsymbol{q}_\mathbf{a}^\mathbf{b} \begin{bmatrix} 0 \\ \mathbf{v_a} \end{bmatrix} \boldsymbol{q}_\mathbf{a}^{\mathbf{b}^{-1}} \tag{2.11}$$

Where $\boldsymbol{q}_\mathbf{a}^{\mathbf{b}^{-1}}$ is the inverse quaternion of $\boldsymbol{q}_\mathbf{a}^\mathbf{b}$.

We can construct the 3×3 rotation matrix to perform the rotation in a single matrix multiply operation. This rotation matrix in terms of quaternion elements is:

$$\boldsymbol{R}_b^e = \begin{bmatrix} q_0^2 + q_1^2 + q_2^2 - q_3^2 & 2q_1q_2 - 2q_0q_3 & 2q_1q_3 + 2q_0q_2 \\ 2q_1q_2 + 2q_0q_3 & q_0^2 - q_1^2 + q_2^2 - q_3^2 & 2q_2q_3 - 2q_0q_1 \\ 2q_1q_3 - 2q_0q_2 & 2q_2q_3 + 2q_0q_1 & q_0^2 - q_1^2 - q_2^2 + q_3^2 \end{bmatrix} \tag{2.12}$$

And then Euler angles can be derived:

$$\begin{aligned} \tan\phi &= \frac{2(q_0q_1 + q_2q_3)}{1 - 2(q_1^2 + q_2^2)} \\ \sin\theta &= 2(q_0q_2 - q_1q_3) \\ \tan\psi &= \frac{2(q_0q_3 + q_1q_2)}{1 - 2(q_2^2 + q_3^2)} \end{aligned} \tag{2.13}$$

By considering that Euler angles' value ranges are $\psi \in [-\pi, \pi]$, $\theta \in [-\pi/2, \pi/2]$, $\phi \in [-\pi, \pi]$, the solutions to these three equations are:

$$\begin{aligned} \phi &= \arctan\frac{2(q_0q_1 + q_2q_3)}{1 - 2(q_1^2 + q_2^2)} \\ \theta &= \arcsin\left(2(q_0q_2 - q_1q_3)\right) \\ \psi &= \arctan\left(\frac{2(q_0q_3 + q_1q_2)}{1 - 2(q_2^2 + q_3^2)}\right) \end{aligned} \tag{2.14}$$

2.5.4 Remarks on transformations of reference frames

- The transformations do not alter the vector in either magnitude or spatial orientation, it is physically the same vector but expressed in different coordinate systems.
- In flight mechanics, it is habitual to use a sequence of angular rotations following the Euler angle technique. Equations of motion using quaternions are also common; those using DCM are rare [28].
- The Euler angle singularity at 90 degrees is avoided by the use of either quaternions or by direction cosines. However, they have the disadvantage of lacking the intuitive feel as aircraft attitude coordinates. Flight dynamics time histories calculated with quaternions or DCM needed to be translated into Euler angles for intelligent use [28].

2.6 System modeling

Various mathematical models for quadcopter aircrafts exist in literature with several differences:

- They vary in the modelling approach, which is either
  1- Euler-Newton formalism
  2- Lagrangian formalism.

- They vary in the number of forces and moments taken into account, i.e. degree of simplification of the real model.

- They vary in the orientation of the body coordinate system, most of the papers choose the body axes orientation to be along the arms of the vehicle, and the direction of the z_b axis to point upwards.

We'll follow the methods described in [24]. because of its simplicity and the inclusion of a minimum number of states and inputs. And since both formalisms generate the same results, we'll describe only the Lagrangian formalism.

The quadcopters movements and axes are defined in the next figure:

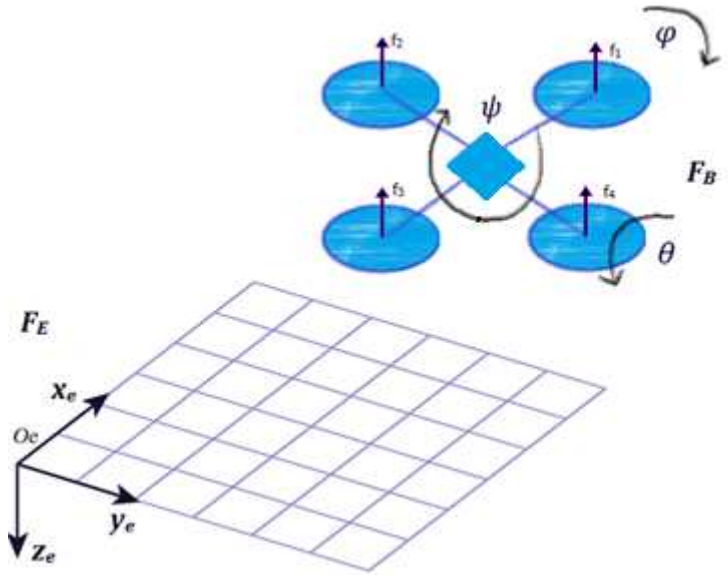

Figure 2.5 Definition of the movements and axes.

2.6.1 Simplifying assumptions

Simplifying assumptions are included in the model to simplify the analysis as much as possible, while maintaining meaningful and reasonable physical results. We will assume the following to our model:

- The quadcopter is a solid-body structure.
- The CG and the body-fixed frame origin are assumed to coincide.
- Thrust and drag are proportional to the square of propeller's speed.

2.6.2 The Euler-Lagrange formalism

This method is based on energy and kinematics, where we introduce the Lagrangian function $L = T - U$. where T and U are the kinetic and the potential energy respectively.

Let $\boldsymbol{q} = (x, y, z, \psi, \theta, \varphi)^{\mathrm{T}} \in \mathbb{R}^6$ represent the generalized coordinates of the rotorcraft. (x, y, z) denote the position of the centre of mass of the rotorcraft with respect the frame $\mathrm{F_e}$, and $\boldsymbol{\eta} = (\psi, \theta, \varphi)$ are the three Euler angles: yaw, pitch and roll, always in $\mathrm{F_E}$. Define the translational and rotational variables respectively $\boldsymbol{\xi} = (x, y, z)^{\mathrm{T}}$ and $\boldsymbol{\eta} = (\psi, \theta, \varphi)^{\mathrm{T}}$.

The translational kinetic energy of the rotorcraft is:

$$T_{trans} \triangleq \frac{m}{2}\dot{\boldsymbol{\xi}}^{\mathrm{T}}\dot{\boldsymbol{\xi}} \tag{2.15}$$

where m denotes the mass of the rotorcraft.

The rotational kinetic energy is:

$$T_{rot} \triangleq \frac{1}{2}\boldsymbol{\Omega}^{\mathrm{T}}\boldsymbol{I}\,\boldsymbol{\Omega} \tag{2.16}$$

Where $\boldsymbol{\Omega}$ is the vector of the angular velocity $\boldsymbol{\Omega} = \begin{bmatrix} p \\ q \\ r \end{bmatrix}$ and $\boldsymbol{I}$ is the (constant) inertia matrix:

$$\boldsymbol{I} = \begin{bmatrix} Ixx & 0 & 0 \\ 0 & Iyy & 0 \\ 0 & 0 & Izz \end{bmatrix} \tag{2.17}$$

The angular velocity vector $\boldsymbol{\Omega}$ resolved in the body-fixed frame is related to the generalized velocities $\dot{\boldsymbol{\eta}}$ by means of the standard kinematic relationship:

$$\boldsymbol{\Omega} = \boldsymbol{W}_{\eta}\dot{\boldsymbol{\eta}} \tag{2.18}$$

Where the matrix $\boldsymbol{W}_{\eta}$ is the matrix that converts Euler angular rates to aircraft angular rates, which is the inverse transformation of that given in appendix A.2 (if we inverse $\boldsymbol{D}$ we get $\boldsymbol{W}_{\eta}$).
Substituting the equation (2.18) in the equation of rotational kinetic energy gives:

$$T_{rot} \triangleq \frac{1}{2}\,\dot{\boldsymbol{\eta}}^{\mathrm{T}}\boldsymbol{J}\,\dot{\boldsymbol{\eta}} \tag{2.19}$$

Where:

$$\boldsymbol{J} = \boldsymbol{J}(\boldsymbol{\eta}) = \boldsymbol{W}_{\eta}^{\mathrm{T}}\,\boldsymbol{I}\,\boldsymbol{W}_{\eta} \tag{2.20}$$

The matrix $\boldsymbol{J}$ acts as the inertia matrix for the full rotational kinetic energy of the rotorcraft expressed directly in terms of the generalized coordinates $\boldsymbol{\eta}$.

The gravitational potential is given by:

$$U = mgz \tag{2.21}$$

The Lagrangian function is:

$$L(q,\dot{q}) = T_{trans} + T_{rot} - U$$

$$= \frac{m}{2}\dot{\boldsymbol{\xi}}^{\mathrm{T}}\dot{\boldsymbol{\xi}} + \frac{1}{2}\dot{\boldsymbol{\eta}}^{\mathrm{T}}\boldsymbol{J}\dot{\boldsymbol{\eta}} - mgz \tag{2.22}$$

And the general form of the equations of motion in Lagrange method is:

$$\frac{d}{dt}\left(\frac{\partial L}{\partial \dot{\boldsymbol{q}}}\right) - \frac{\partial L}{\partial \boldsymbol{q}} = \begin{pmatrix}\boldsymbol{F}_{\xi}\\ \boldsymbol{\tau}\end{pmatrix} \tag{2.23}$$

Where $\boldsymbol{\tau}$ is the generalized moments and $\boldsymbol{F}_{\xi}$ is the translational force applied to the rotorcraft due to the control inputs:

$$\boldsymbol{F}_{\xi} = \boldsymbol{R}_{\mathrm{b}}^{\mathrm{e}}\,\widehat{\boldsymbol{F}} \tag{2.24}$$

$\widehat{\boldsymbol{F}}$ is he thrust vector:

$$\widehat{\boldsymbol{F}} = \begin{pmatrix}0\\0\\u\end{pmatrix} \tag{2.25}$$

where u is the main thrust directed out of the bottom of the aircraft and expressed as:

$$u = \sum_{i=1}^{4} f_i \tag{2.26}$$

Each motor Mi produces a thrust force f_i which is proportional to the square of the angular speed, that is given that the quad-rotor's motors can only turn in a fixed direction, the produced force f_i is always positive.

$$f_i = kw_i^2 \tag{2.27}$$

The generalized moments on the $\boldsymbol{\eta}$ variables are:

$$\boldsymbol{\tau} = \begin{pmatrix}\tau_{\psi}\\ \tau_{\theta}\\ \tau_{\phi}\end{pmatrix}$$

Where

$$\begin{aligned} \tau_{\psi} &= \sum_{i=1}^{4} \tau_{Mi} \\ \tau_{\theta} &= (f_{2-} f_4)\ell \\ \tau_{\phi} &= (f_{3-} f_1)\ell \end{aligned} \tag{2.28}$$

Since the Lagrangian contains no cross terms in the kinematic energy combining $\dot{\xi}$ with $\dot{\eta}$, the Euler–Lagrange equation can be partitioned into dynamics for ξ coordinates and η coordinates.

The Euler–Lagrange equation for the translational motion is:

$$\frac{d}{dt}\left(\frac{\partial L_{tran}}{\partial \dot{\boldsymbol{\xi}}}\right) - \frac{\partial L_{tran}}{\partial \boldsymbol{\xi}} = \boldsymbol{F}_{\xi} \tag{2.29}$$

Then:

$$m\ddot{\boldsymbol{\xi}} + m\, g\, \mathbf{z}_{\mathrm{e}} \;=\; \boldsymbol{F}_{\xi} \tag{2.30}$$

As for the η coordinates, it can be written

$$\frac{d}{dt}\left(\frac{\partial L_{rot}}{\partial \dot{\boldsymbol{\eta}}}\right) - \frac{\partial L_{rot}}{\partial \boldsymbol{\eta}} = \boldsymbol{\tau} \tag{2.31}$$

We obtain:

$$\boldsymbol{J}\ddot{\boldsymbol{\eta}} + \dot{\boldsymbol{J}}\dot{\boldsymbol{\eta}} - \frac{1}{2}\frac{\partial}{\partial \boldsymbol{\eta}}(\dot{\boldsymbol{\eta}}^{\mathrm{T}}\boldsymbol{J}\dot{\boldsymbol{\eta}}) = \boldsymbol{\tau} \tag{2.32}$$

We define the Coriolis-centripetal vector

$$\bar{V}(\boldsymbol{\eta}, \dot{\boldsymbol{\eta}}) = \dot{\boldsymbol{J}}\dot{\boldsymbol{\eta}} - \frac{1}{2}\frac{\partial}{\partial \boldsymbol{\eta}}(\dot{\boldsymbol{\eta}}^{\mathrm{T}}\boldsymbol{J}\dot{\boldsymbol{\eta}}) \tag{2.33}$$

(2.32) becomes

$$\boldsymbol{J}\ddot{\boldsymbol{\eta}} + \bar{V}(\boldsymbol{\eta}, \dot{\boldsymbol{\eta}}) = \boldsymbol{\tau} \tag{2.34}$$

But $\bar{V}(\boldsymbol{\eta}, \dot{\boldsymbol{\eta}})$ can be expressed as

$$\bar{V}(\boldsymbol{\eta}, \dot{\boldsymbol{\eta}}) = \left(\dot{\boldsymbol{J}} - \frac{1}{2} \frac{\partial}{\partial \boldsymbol{\eta}} (\dot{\boldsymbol{\eta}}^{\mathrm{T}} \boldsymbol{J}) \right) \dot{\boldsymbol{\eta}} \tag{2.35}$$
$$= C(\boldsymbol{\eta}, \dot{\boldsymbol{\eta}}) \dot{\boldsymbol{\eta}}$$

Where $C(\boldsymbol{\eta}, \dot{\boldsymbol{\eta}})$ is referred to as the Coriolis term and contains the gyroscopic and centrifugal terms associated with the $\boldsymbol{\eta}$ dependence of $\boldsymbol{J}$. This yields

$$m\ddot{\boldsymbol{\xi}} + mg\mathbf{z}_{\mathrm{e}} = \boldsymbol{F}_{\xi} \tag{2.36}$$
$$\boldsymbol{J}\ddot{\boldsymbol{\eta}} = \boldsymbol{\tau} - C(\boldsymbol{\eta}, \dot{\boldsymbol{\eta}})\dot{\boldsymbol{\eta}} \tag{2.37}$$

To simplify let us take

$$\tilde{\boldsymbol{\tau}} = \begin{pmatrix} \tilde{\tau}_{\psi} \\ \tilde{\tau}_{\theta} \\ \tilde{\tau}_{\varphi} \end{pmatrix} = \boldsymbol{J}^{-1}(\boldsymbol{\tau} - C(\boldsymbol{\eta}, \dot{\boldsymbol{\eta}})\dot{\boldsymbol{\eta}}) \tag{2.38}$$

Finally:

$$\begin{aligned} m\ddot{x} &= u(\sin\varphi \sin\psi + \cos\varphi \cos\psi \sin\theta) \\ m\ddot{y} &= u(cos\varphi\ sin\ \theta\ sin\psi\ - cos\psi\ sin\ \varphi) \\ m\ddot{z} &= u\ cos\ \theta\ cos\varphi\ - mg \\ \ddot{\psi} &= \tilde{\tau}_{\psi} \\ \ddot{\theta} &= \tilde{\tau}_{\theta} \\ \ddot{\varphi} &= \tilde{\tau}_{\varphi} \end{aligned} \tag{2.39}$$

Where x and y are coordinates in the horizontal plane, z is the vertical position, and $\tilde{\tau}_{\psi}$, $\tilde{\tau}_{\theta}$ and $\tilde{\tau}_{\varphi}$are the yawing moment, pitching moment and rolling moment, respectively, which are related to the generalized torques τ_{ψ}, τ_{θ} and τ_{φ}.

3 Design of the Quadcopter Platform

Chapter 3 Introduction

This chapter is dedicated to the design stage, we we'll explore the basic steps of this stage where we start by the choice of material, which is a major consideration because the structure should offer a good rigidity while being as light as possible. The next step is dimensioning the structural parts and assembling them to build the CAD model. After that, We set up a static study to simulate our quadcopter in the worst case scenario of climbing vertically with a high vertical acceleration.

We will start by the study of an exemplary design project, it's a doctoral project by an Algerian researcher, which aimed to methodologically build an optimised quadcopter.

How the quadcopter airframe is designed and analysed?

3.1 The design considerations

Designing a quadcopter is basically dealing with numerous design parameters that are closely linked. Taking a decision about all these parameters requires a clear methodology. The design should take into consideration the proprieties of the components and their interactions, or the assembled multicopter may have poor performance, or even could not work at all. For example, a span that is too small may cause the propellers to touch each other while rotating.

The body should also have good dampening characteristics as vibrations can affect the performance of the accelerometer and gyroscope, plus the video quality will be damaged. Some materials are excellent at dampening vibrations like carbon fibre for example.

3.2 Case study: the design of the OS4

The work of S. Bouabdellah [29] on the OS4 research-purpose quadcopter, which he started in 2003, is an exemplary design project. The design method was determined by the application of the vehicle, which was autonomous flying .This method combined the theoretical knowledge and the results of a system level optimization analysis which allowed to select —using iterative algorithms— the best components in list of options, rather than the direct choice. The project was also accompanied by the construction of a test bench with off-board data processing and power supply. It was used to safely and easily test control strategies.

The design process started by setting three constraints from the application definition: maximum mass $m_{\max}$, maximum span $s_{\max}$ and target thrust/weight ratio β. The value of propeller diameter d_{prop} could be supposed from $s_{\max}$. Then using d_{prop}, the characteristics of the propeller were estimated in term of thrust, drag and power. The motor power requirements can then be fully defined using the mass $m_{\max}$, the drag moment produced by the propellers and the thrust/weight ratio. An iterative algorithm selects from a database a list of candidate motors which offered the required power.

Simultaneously, a rough estimation of the mass of the airframe m_{af} and avionics m_{av} was made to have a first estimation of the total mass without battery. the iterative algorithm had to find m_{pg} and m_{bat} , as described in figure 3.1 [29].

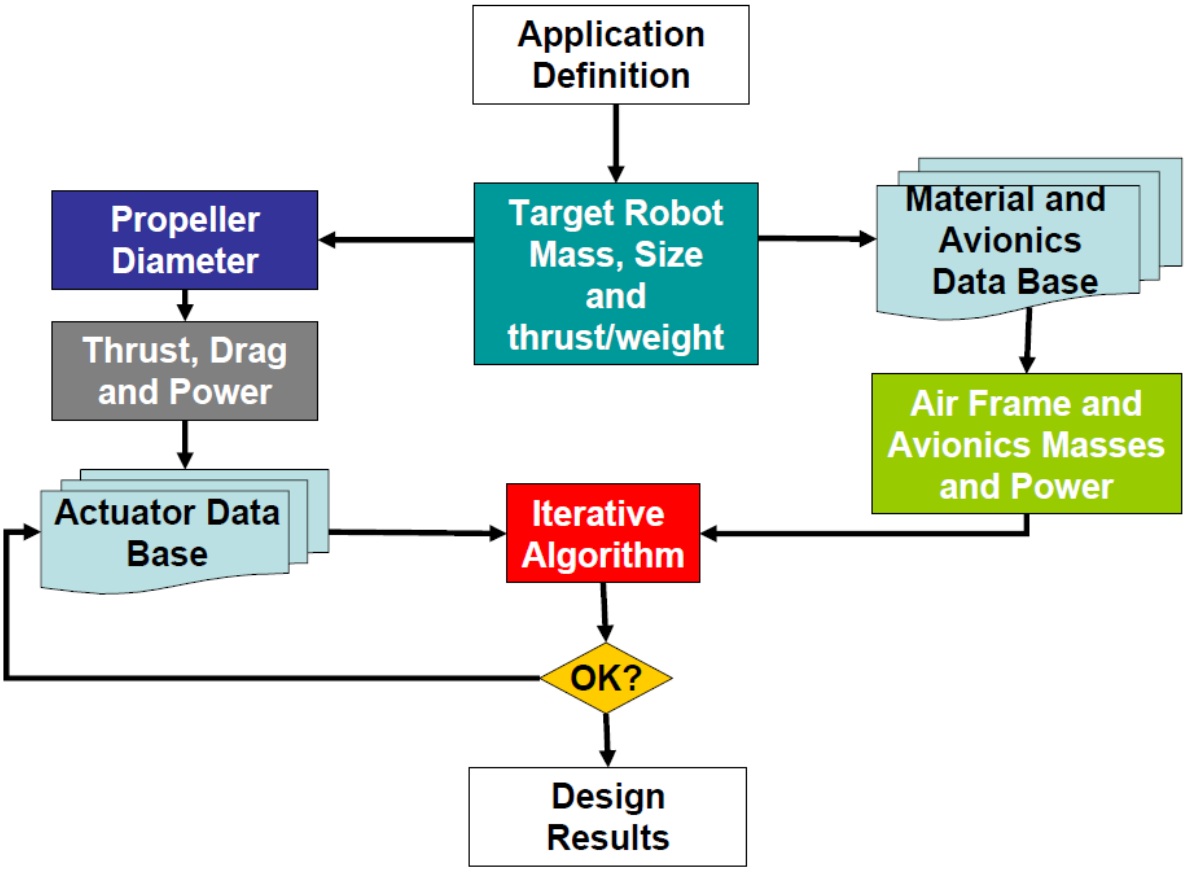

Figure 3.1 The design method flowchart of the OS4 [29].

In addition to standard physics equations and electrical DC motor formulas, this algorithm considered several factors proposed by the author, such as Propulsion Group Cost Factor; Propulsion Group Quality Factor; Autonomy and the Design Quality Index.

The initial constraints for this optimization program were:

$$m_{\max} = 500g$$
$$s_{\max} = 800mm$$
$$\beta = 2$$

After an initial design was constructed, several mechanical and electrical parts were added in order to reinforce the structure or add functionalities. Eventually, the mechanical and geometrical characteristics of this quadcopter were:

3.2.1 Mass

The total mass was:

$$m = 650\ g$$

Which is divided as follows:

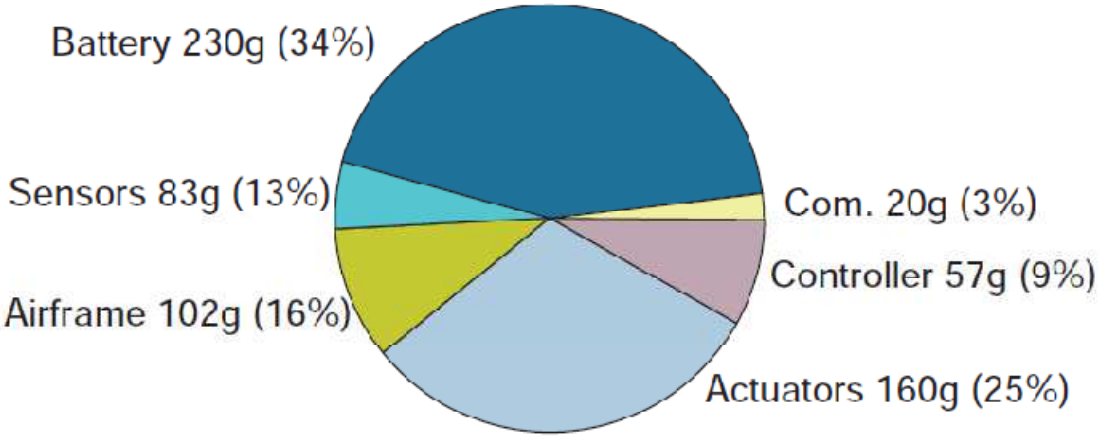

Figure 3.2 Mass distribution of the OS4 [29].

3.2.2 Geometry

- Span:

$$s = 772\text{mm}$$

- propeller radius:

$$R_{rad} = 150\text{mm}$$

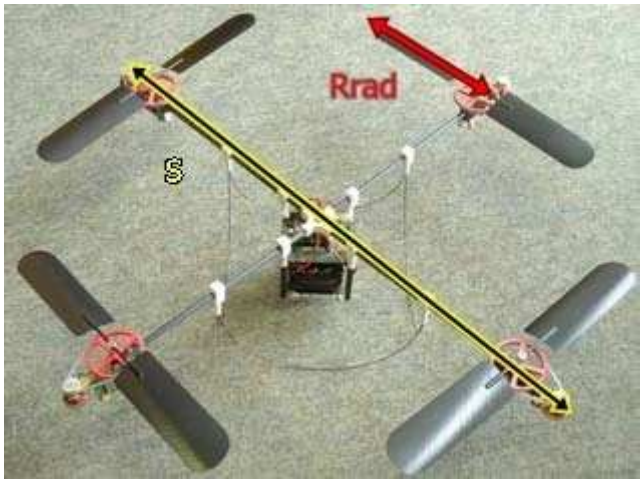

Figure 3.3 Geometry of the OS4.

3.2.3 Propulsion Group

- Motor : LRK 195.03 brushless DC motor (12 g, 35W)
- Gearbox: a gearbox was added because a direct-drive propulsion group allowed only a thrust/weight ratio of $\beta = 0.75$, which was obviously not enough to lift the robot. The reduction ratio of the gearbox was 4:1.
- Thrust margin : 53%

3.3 The design of the quadcopter airframe

In this work we will design a quadcopter platform, a platform or an airframe is the physical structure that supports the quadcopter, it carries the components and the payload. The quadcopter platform should create a strong body to support the stresses generated by external forces and torques while being as light as possible.

Our quadcopter will be of the micro category (the mass should not exceed 1 kg), and a payload of 150 g is envisaged, this is the typical mass of a smartphone or a digital camera, which opens the way for numerous possible uses.

The airframe material should minimise the construction costs while having good mechanical characteristics. Various construction materials exist with their own advantages and disadvantage, materials such as plastic, carbon fibre, aluminium and wood were used in previous existing research. Wood is our best option since it is obtainable and it combines strength and low cost.

3.3.1 Numerical modelling and simulation

We will use Ansys for numerical modelling and simulation (Ansys Academic Student 2020 R1), where we will perform a static structural study using FEM analysis, the goal is to obtain the stress field and the displacement field.

The Ansys Workbench analysis tool comprises several building blocks called *systems*, each system has one or more components called *cells*. We will use the *Static Structural* system. Then, using the cells in this system we will define analysis characteristics such as material properties, geometry dimensions, and boundary conditions.

3.3.1.1 Material properties definition

First we will define the proprieties of the material that we will use to construct the real model. Wood is a complex structure, not only it is orthotropic, but it is cylindrically orthotropic, it has three axes of material symmetry corresponding to longitudinal (L), radial (R) and transverse (T) directions, the reference axis system relates to positions within the tree stem from which any particular piece of wood was cut, with the L axis coinciding with the fibre direction, as depicted in figure 3.4.

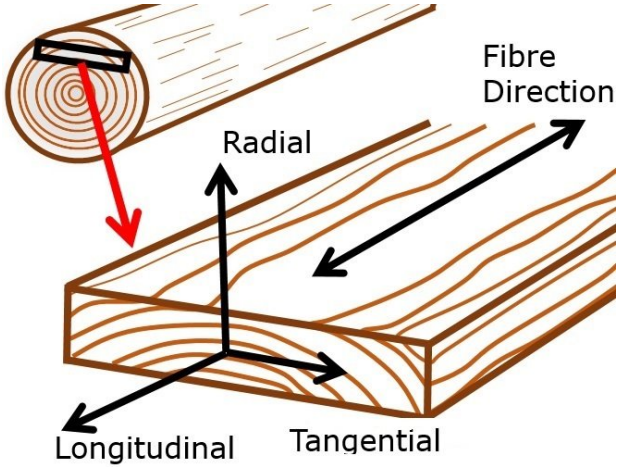

Figure 3.4 The three orthotropic axes of wood material.

The material is presumed rectilinearly orthotropic, this amounts to assuming the value of the radial coordinate is large, i.e., the wood is cut well away from the central pith [30].

Wood species are very different in terms of mechanical proprieties. The species we will use is Scots Pine wood which have the following elastic constants [31]:

Table 3.1 Values of elastics constants of the chosen wood species.

Density kg/m³	E_L MPa	E_R MPa	E_T MPa	ν_{TR} -	ν_{LR} -	ν_{RT} -	ν_{LT} -	ν_{RL} -	ν_{TL} -	G_{LT} MPa	G_{LR} MPa	G_{TR} MPa
550	16300	1100	570	0.68	0.038	0.31	0.015	0.42	0.51	680	1160	66

For an orthotropic material, the elastic constitutive relations for a constant temperature can be expressed as [32]:

$$\begin{bmatrix}\sigma_1\\ \sigma_2\\ \sigma_3\\ \sigma_4\\ \sigma_5\\ \sigma_6\end{bmatrix}=\begin{bmatrix}Q_{11} & Q_{12} & Q_{13} & 0 & 0 & 0\\ Q_{12} & Q_{22} & Q_{23} & 0 & 0 & 0\\ Q_{13} & Q_{23} & Q_{33} & 0 & 0 & 0\\ 0 & 0 & 0 & 2Q_{44} & 0 & 0\\ 0 & 0 & 0 & 0 & 2Q_{55} & 0\\ 0 & 0 & 0 & 0 & 0 & 2Q_{66}\end{bmatrix}\begin{bmatrix}e_1\\ e_2\\ e_3\\ e_4\\ e_5\\ e_6\end{bmatrix} \tag{3.1}$$

Where:

σ_i $(i = 1-6)$ are the 6 general strain components.

Q_{ij} $(i,j = 1-6)$ are the 9 independent elastic parameters for orthotropic materials.

e_i $(i = 1-6)$ are the 6 general stress components.

This material isn't pre-included in the engineering data so we will define our elasticity model by entering the elastic parameters in the material stiffness matrix $\boldsymbol{Q}$.

This stiffness matrix is always symmetric, and its elements of are given by:

$$\begin{gathered}Q_{11} = E_{11}(1-\nu_{23}\nu_{32})/\Delta\\ Q_{22} = E_{22}(1-\nu_{31}\nu_{13})/\Delta\\ Q_{33} = E_{33}(1-\nu_{12}\nu_{21})/\Delta\\ Q_{12} = E_{22}(\nu_{12}+\nu_{32}\nu_{13})/\Delta\\ Q_{13} = E_{33}(\nu_{13}+\nu_{12}\nu_{23})/\Delta\\ Q_{23} = E_{33}(\nu_{23}+\nu_{21}\nu_{13})/\Delta\\ Q_{44} = G_{23}\\ Q_{55} = G_{13}\\ Q_{66} = G_{12}\\ \Delta \equiv 1-\ \nu_{12}\nu_{21}-\nu_{23}\nu_{32}-\nu_{13}\nu_{31}-2\nu_{21}\nu_{32}\nu_{13}\end{gathered} \tag{3.2}$$

Using the elastic constants in table 3.1, the values of the matrix coefficients are (in MPa):

$$Q_{11} = 16992.8$$

$$Q_{22} = 1441.9$$

$$Q_{33} = 740.9$$

$$Q_{12} = 70$$

$$Q_{13} = 20.2$$

$$Q_{23} = 238.2$$

$$Q_{44} = 66$$

$$Q_{55} = 680$$

$$Q_{66} = 1160$$

We insert these values in the Engineering Data cell:

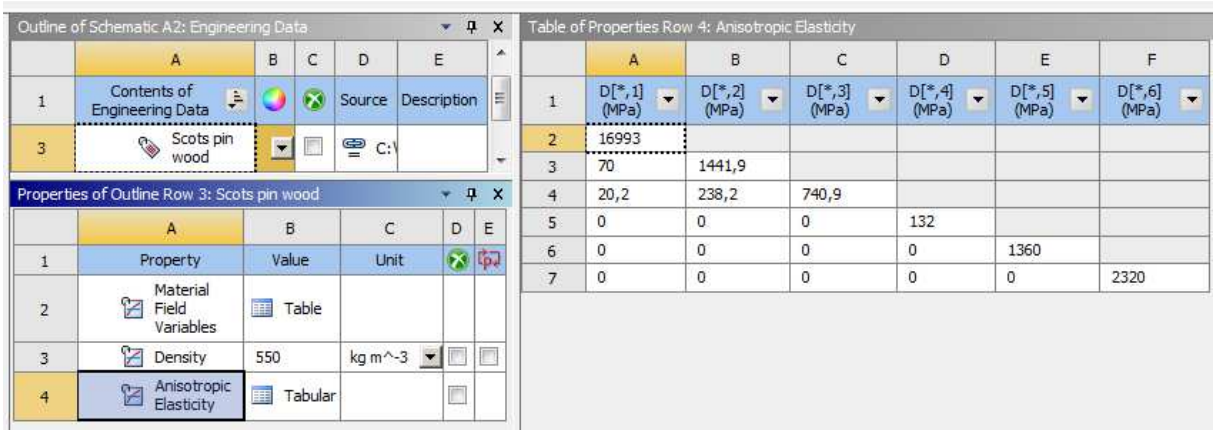

Figure 3.5 Entering the values of the stiffness matrix in the program.

The directions of the orthotropic material are defined according the local coordinate system assigned to each piece, the material directions L, R and T will be aligned with the local x, y and z axes.

3.3.1.2 Geometry creation

The airframe is basically a central square ring on which four beams are fixed, the dimensions of the square are given in figure 3.6.

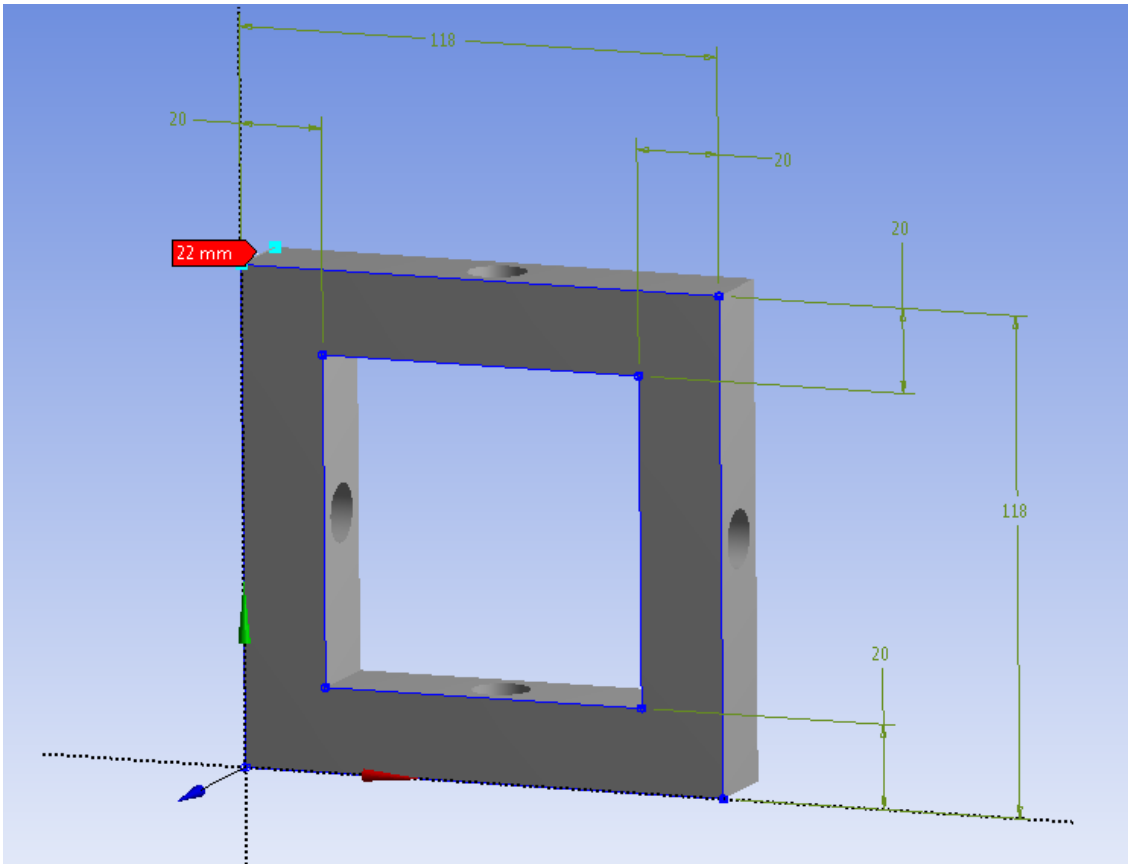

Figure 3.6 Dimensions of the central square (mm).

The four arms of the quadcopter are 16x16 mm and they are 255 mm long each. They attach to the square through circular openings of 14 mm diameter. We assemble the entire frame by defining joints connections type which is a fixed joint that immobilise all DOFs (see figure 3.7).

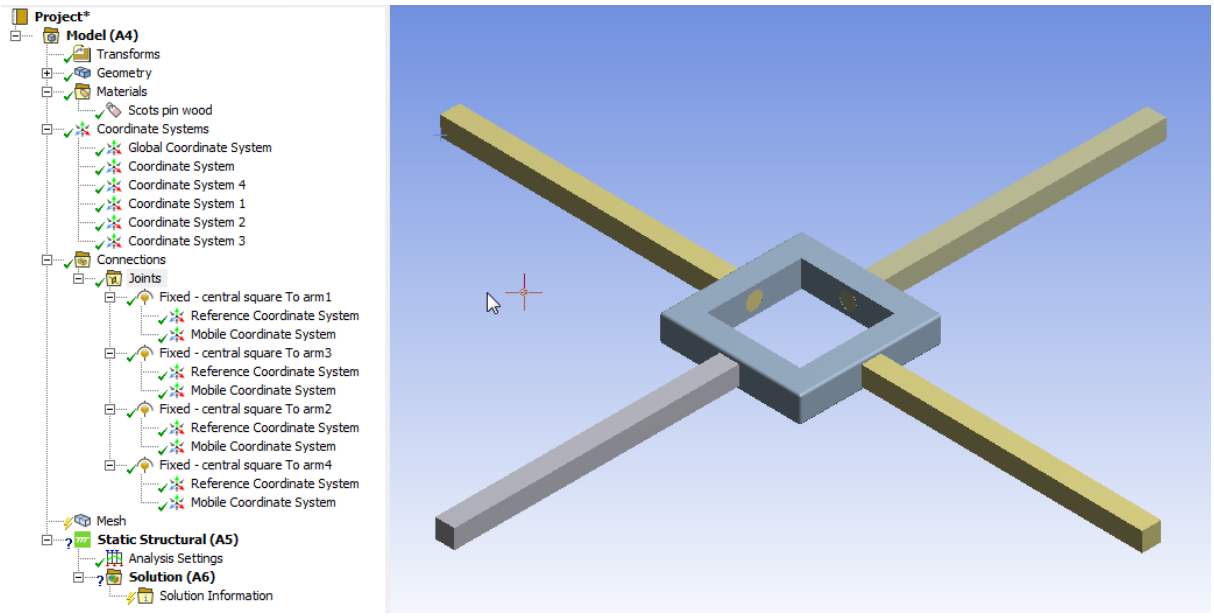

Figure 3.7 Assembled quadcopter and the joint type.

3.3.1.3 Boundary conditions

To define the boundary conditions we make an estimation of the quadcopter total weight, we set it to be 900g (this includes motors, propellers, , battery, electronics and the airframe).

Assuming the quadcopter would be able to achieve its maximum rate of climb of 5m/s in 1 second – this is equal to an acceleration of 5m/s2. The inertial effects are due to this constant vertical acceleration and also to the acceleration of gravity, The 4 propellers will have to equalise the inertia of the quadcopter, if we set $g = 9.81\ N/kg$ then the force of each motor would be:

$$f_i = \frac{0.9*(9.81+5)}{4} = \frac{0.9*(14.81)}{4} = 3.33225N\ (i = 1-4) \quad (3.3)$$

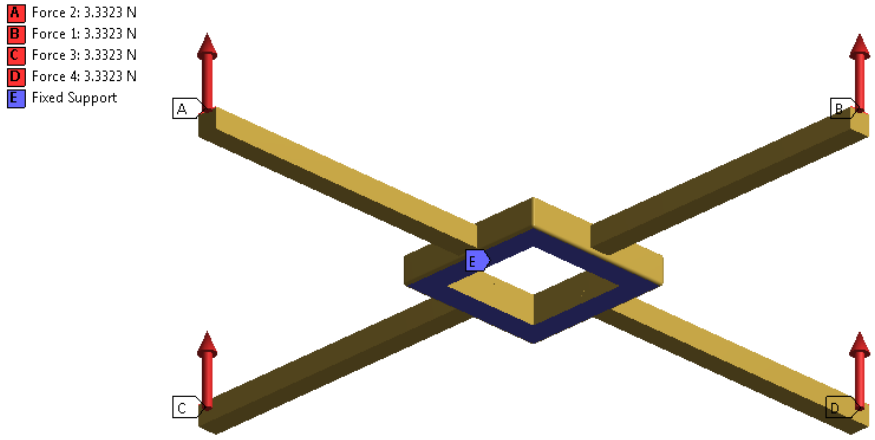

Figure 3.8 Boundary conditions of the quadcopter.

As we can see in figure 3.8, the model features symmetric geometry and symmetric loads. In addition we know that the most sensible part is the connection of fixed arm (as any cantilever beam). Accordingly, it is very sufficient to only study one isolated arm which will simplify and accelerate our calculations, the configuration we will analyse is given in figure 3.9.

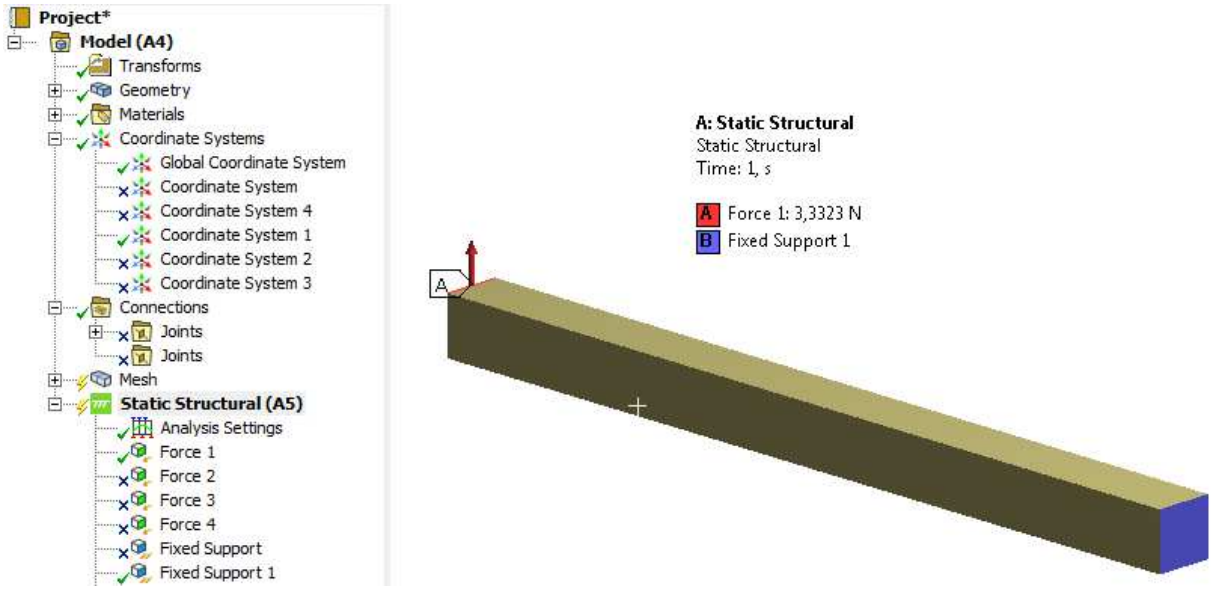

Figure 3.9 Boundary conditions of the isolated arm.

3.3.1.4 Meshing

The maximums stress will determine the resistance of the structure, this maximum will be at the attachment point. Accordingly the mesh will be more refined at that zone.

The mesh is showed in the figure 3.10, we can also see that the orthogonal quality of most of the elements is 1 and skewness is near 0,01, which is a very good index for meshing quality. The main variables introduced in this mesh are listed in table 3.2.

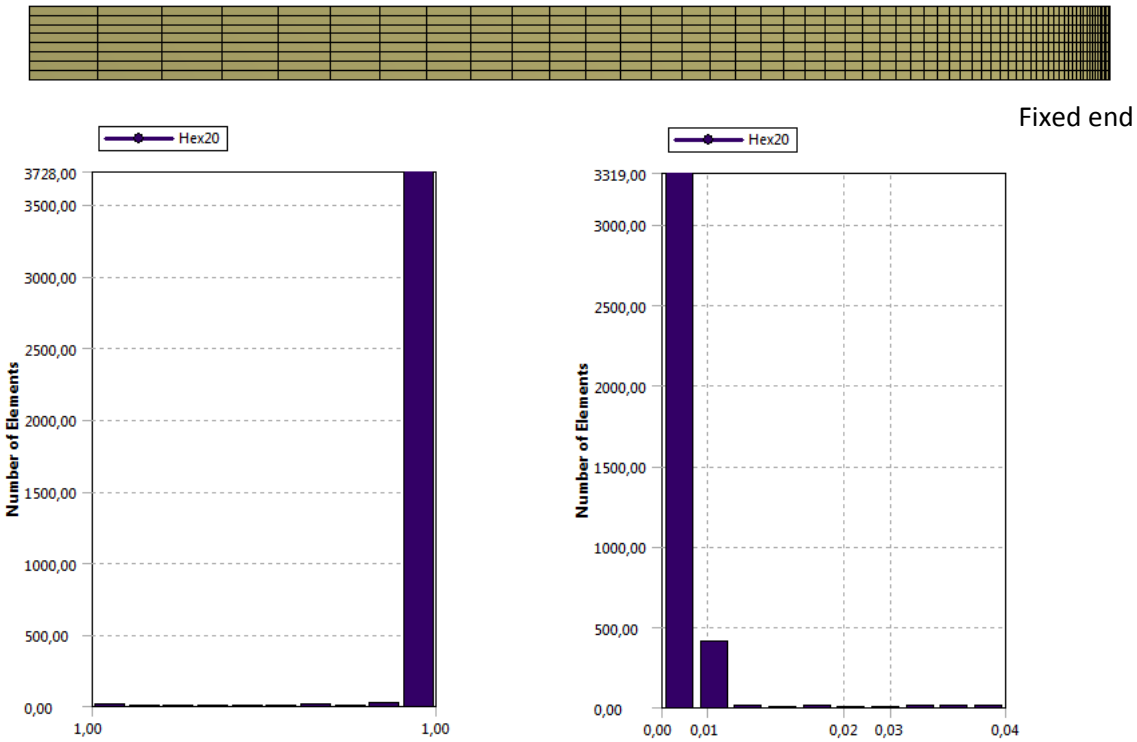

Figure 3.10 Mesh, orthogonal quality (left), and skewness (right).

Table 3.2 Mesh principal proprieties.

Property	Value
Mesh Type	Solid Mesh
Average Skewness	1,2021e-003
Average Orthogonal Quality	0,99998
Characteristic Length	0,38807 mm
Total nodes	18279
Total elements	3776

3.3.2 Results

The first figure shows the displacement field, the maximum displacement was at the free end ($\delta = 0{,}18439\ mm$), then it goes gradually to zero. In the second figure we can see, as expected, that the highest stress occurs immediately at the fixed end (1,3678 MPa), the stress decreases to a minimum of 5,5676e-003 MPa at the free end.

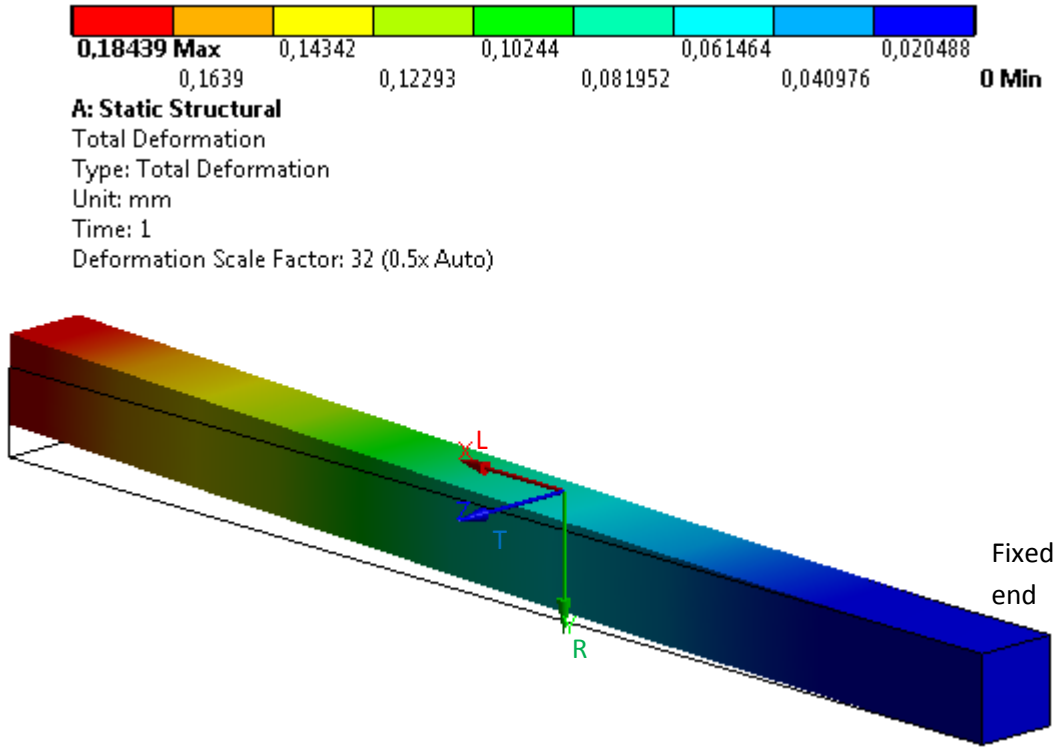

Figure 3.11 Total deformation of the quadcopter arm (mm).

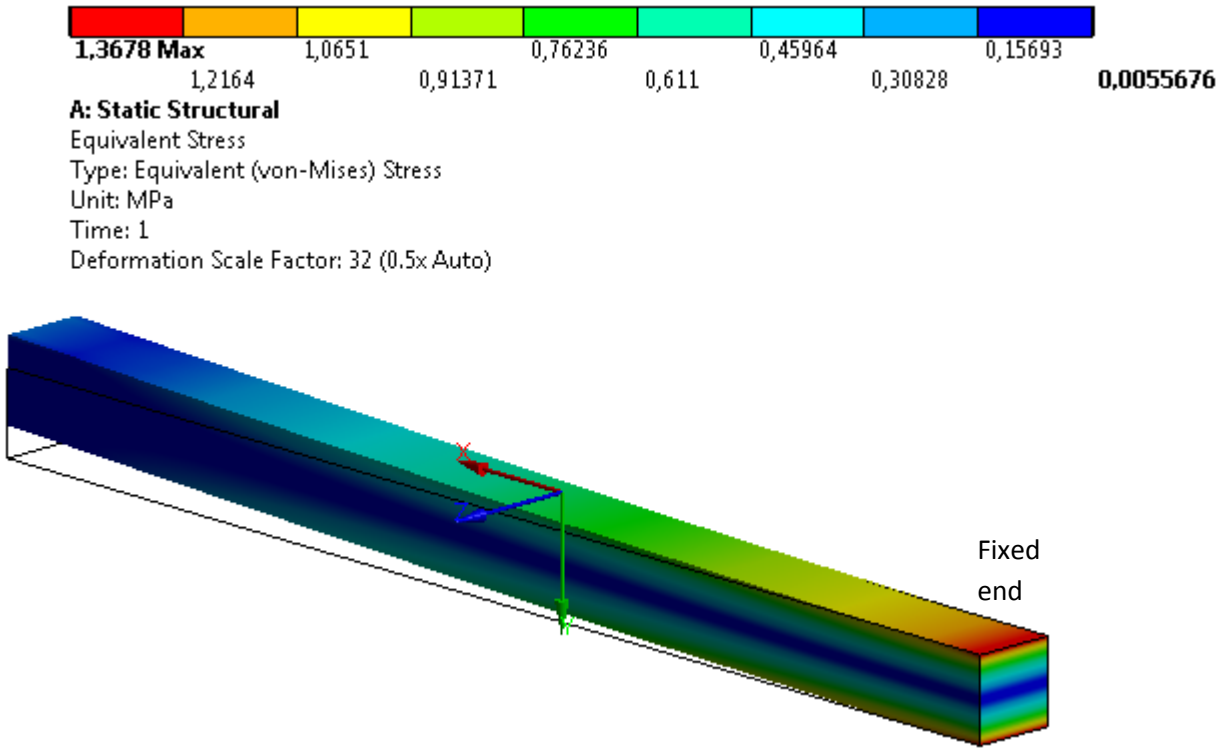

Figure 3.12 Equivalent von-Mises stress of the quadcopter arm (MPa).

We can verify the results of deformation using the empiric formula that gives the free end deflection [33]:

$$\delta = \frac{k_b W L^3}{EI} + \frac{k_s W L}{GA'} \tag{3.4}$$

Where for this configuration, the constants in eq.(3.4) are:

$k_b = \frac{1}{3}$

W is the applied load

L is the beam length

$E = E_L$

I is the moment of inertia $I = bh^3/12$

$k_s = 1$

$G = G_{LT}$

$A' = \frac{5}{6}bh$

Inserting these values in equation (3.4) gives:

$$\delta = 0.16733 \text{ mm}$$

The value of free end deflection calculated by the programme is 0,18439 mm, then the relative difference with respect to the simulation is equal to 0.09.

We note that this is not an exact method but it is an empirical method that take into account only two important elastic constants E_L and G_{LT} and ignore the rest of constants.

For stress, we calculate the bending stress at the upper face where the equivalent stress equals the bending stress, then: $\sigma \mid_{\substack{x=L \\ y=b/2}} = 1{,}1471$ MPa. This gives a relative error of 0,16.

Although the approximations and simplifications, the results were close enough to validate our numerical simulation.

3.3.3 Effect of fibres orientation

Numerical analysis tools offer the possibility to test and analyse different configurations for the same model without building it numerous times and waste time and money in the construction process.

In Ansys we can change the orthotropic directions of an orthotropic body by simply changing the local coordinate system assigned to it. We will retain the same boundary conditions and the same mesh but only change the directions of wood fibres.

The resulting displacement fields and stress fields are showed in figure 3.13 and 3.14 for two different fibre orientations, the X direction is the longitudinal direction of the material, the Y direction is the radial direction and the Z direction is the tangential direction.

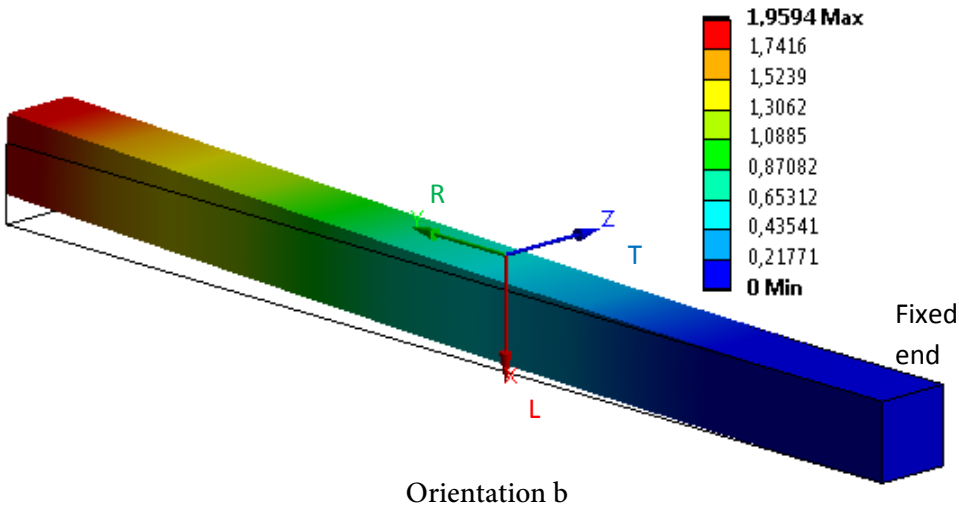

Orientation b

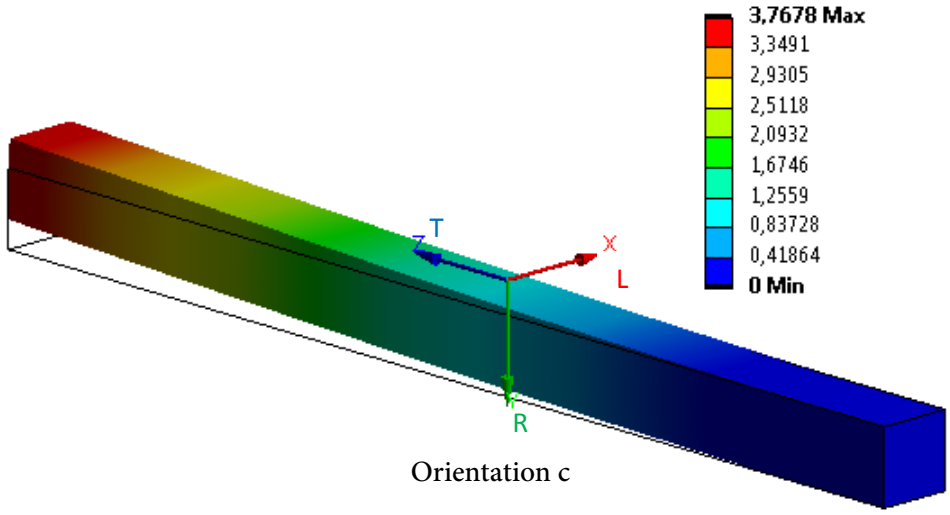

Orientation c

Figure 3.13 Total deformation for fibre orientations b and c (mm).

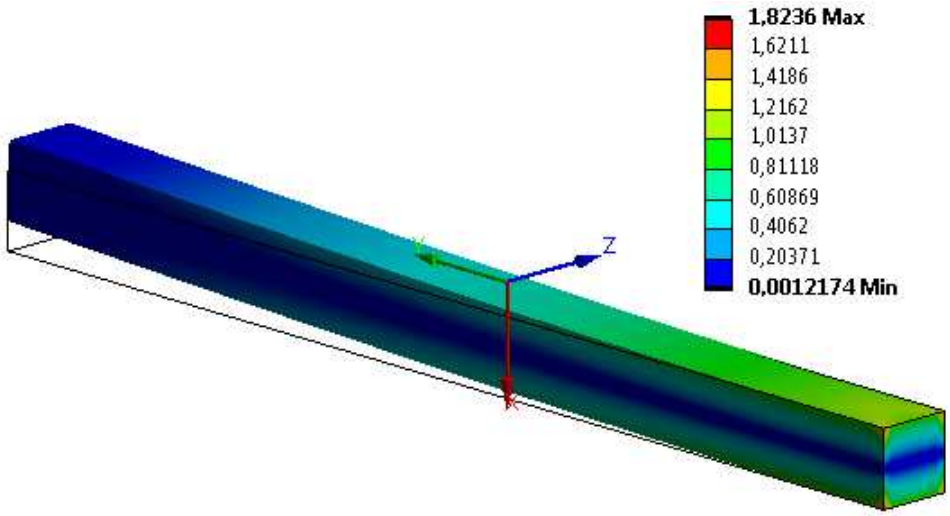

Orientation b

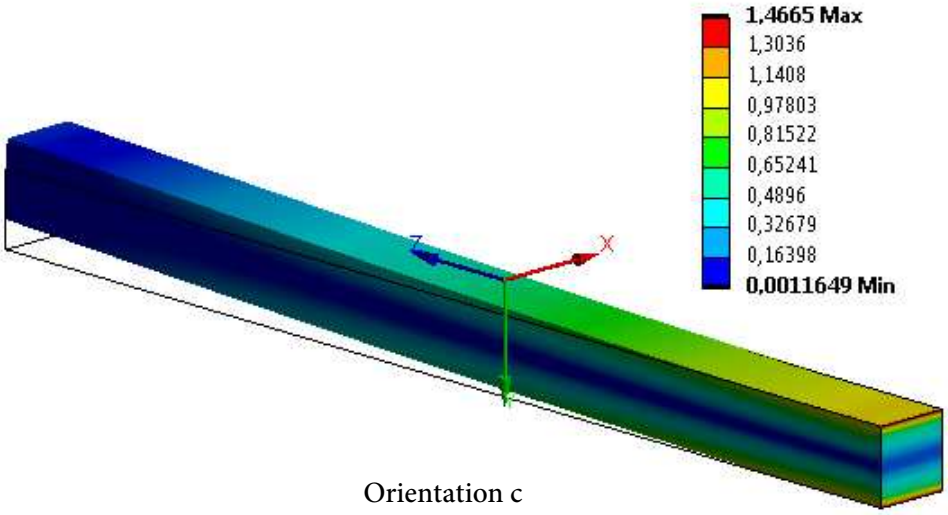

Orientation c

Figure 3.14 Equivalent von-Mises stress for fibre orientations b and c (MPa).

These figures demonstrate that the displacement field vary largely if the orthotropic directions vary. As for the stress field, we didn't see considerable changes except of the pattern of stress near the attachment point. The following table resumes the change of results, the average values are for the entire nodes (8713 nodes). The relative change C_r is provided between brackets to give an idea about the magnitude of the change, the formula for C_r is:

$$C_r = \frac{compared\ value - refernce\ value}{refernce\ value} \tag{3.5}$$

Table 3.3 Average values of deformation and stress for different fibres orientations.

	Deformation [mm]		Stress [MPa]	
	average	max	average	max
Fibres direction a (reference value)	3,0455e-002	0,18439	0,47209	1,3678
Fibres direction b	0,30246 (+893%)	1,9594 (+963%)	0,46891 (-0,7%)	1,8236 (+33%)
Fibres direction c	0,57785 (+1797%)	3,7678 (+1943%)	0,47042(-0.4%)	1,4665 (+7%)

We can see from these data that changing the fibres direction induces a great change in the deflection of the arm, which ranged from +893% to +1943% for cases a and b. On the other hand the stress had a negligible relative change.

Figures 3.15 and 3.16 illustrates the values of this table. The deformation of the beam was greatly higher than the reference direction (when the fibres where aligned with the longitudinal axis). The stress however didn't see any considerable change.

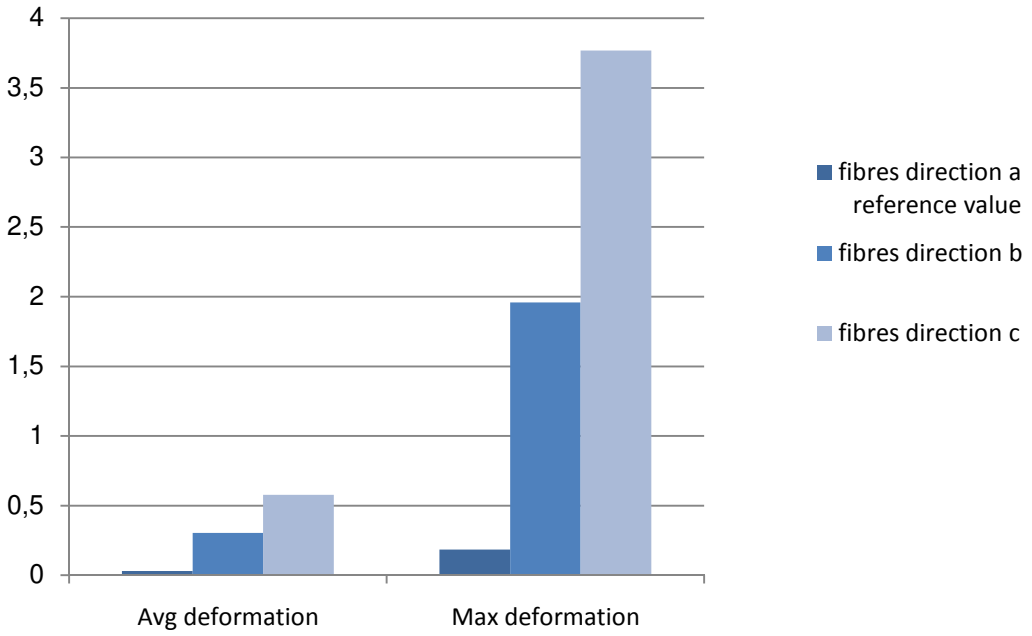

Figure 3.15 Comparison of deformation values for the three fibre orientations (mm).

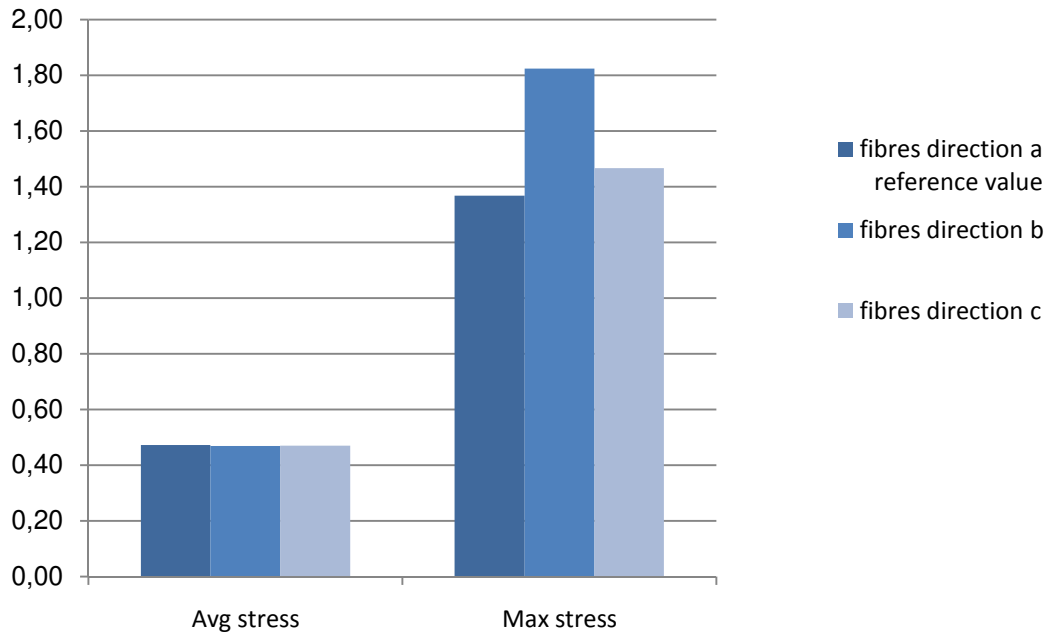

Figure 3.16 Comparison of stress values for the three fibre orientations (MPa).

3.3.4 Discussion of results and conclusion

In this finite elements analysis we tested our platform under extreme conditions (fast climb). It appeared that the most vulnerable part of the quadcopter in terms of mechanical stresses is the connection point between the arm and the body frame.

The displacement field indicated a maximum deflection at the loaded end, while the zone just before the fixed end was not deformed, this is because a fixed joint blocks all DOFs. In addition, the maximum stress was located around the lower and upper faces of the arm and especially near the fixed end, this is because the compressive and tensile stresses always increase the further we go from the neutral plane of the beam, these results are similar to any beam under bending. In our case the upper fibres are under compression and the lower fibres are under tension.

We also remarked that changing the direction of wood fibres had a great impact on the deflection of the arm, the deflection increased largely when the fibres direction (L direction) was not aligned with the longitudinal axis of the beam, and the percentage change was of the order of 10^3%. We can conclude that fibre direction is a very important factor in the rigidity of orthotropic beams and that the most rigid configuration is when the fibres are aligned with

the longitudinal axis of the beam. We remarked also that the stress field had a negligibly small difference which proves that changing the fibres orientation doesn't affect the state of stress.

Finally, given that the Modulus of rupture is 88.9 GPa, and that the maximum stress was far lower from that value, we can conclude that the arm may operate safely without rupture.

3.4 Difficulties encountered during the design

Concerning the difficulties that we encountered during the simulation stage, the most important one was material modelling. Our material was not a conventional isotropic material that can be characterised by 3 values for the E, G and ν, but it was by a matrix that requires the calculation of 9 parameters. Finding the elastic constants included in these parameters required a full research in wood literature, which we eventually found in only one source.

Another difficulty was defining the boundary conditions and the connections between parts. This is because Ansys requires manual configurations to define these conditions, and all this work is the responsibility of the user to learn and accomplish.

The last difficulty was meshing the model, this part was complex because the meshing procedure includes several variables that need to be regulated in order to get a satisfactory quality to capture the physics of the model.

4 Construction of the Quadcopter Platform

Chapter 4 Introduction

This final chapter demonstrates the construction phase of the design. The platform geometry will be the same as that of the CAD model and it will be carefully assembled to assure symmetry and mass equilibrium, which is essential as it makes easier the control and reduces vibrations.

How the quadcopter airframe is constructed?

4.1 Material

Wood will be used for the airframe as it has the quality of workability, that means it is capable of being worked easily by hand or by machines. It is also widely available so in case of loss or damage to the worked piece, a replacement is possible without any significant cost.

4.2 Main frame

The main frame is intended to be of a single block (figure 4.1), this was purposely preferred over the assembly of several parts because it gives better rigidity to the aircraft. The challenge is that this type of design is more difficult to realise than the assembly.

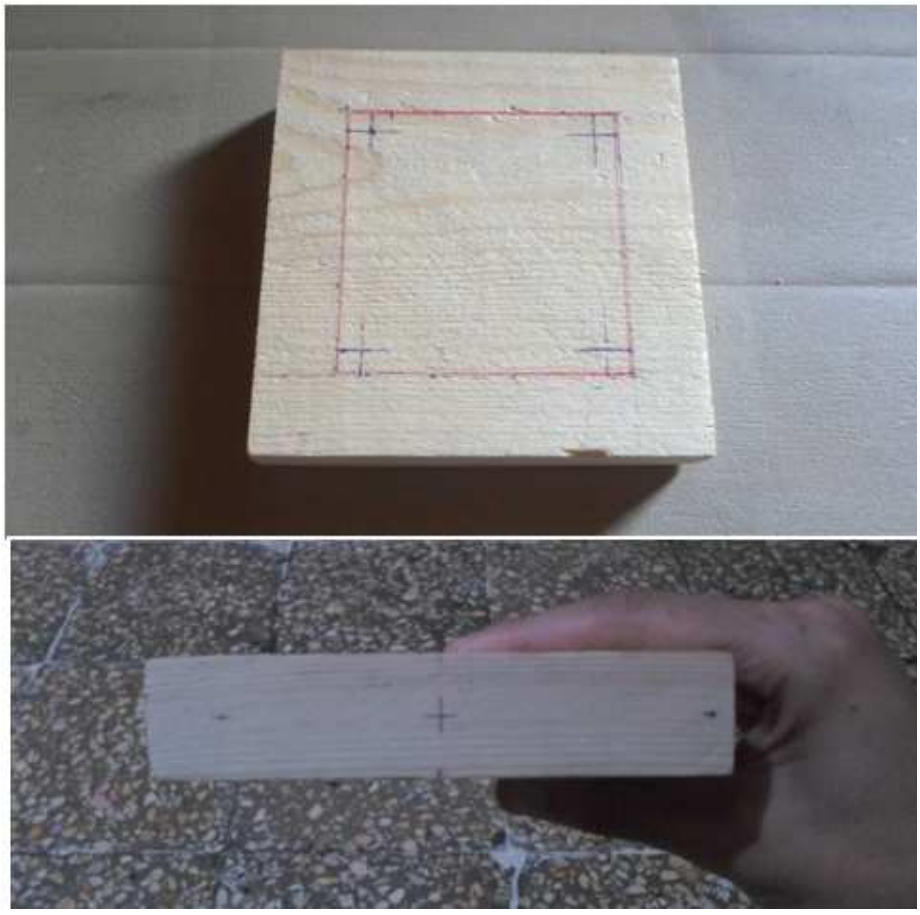

Figure 4.1 Main frame block.

This piece will be worked to be as the CAD piece. The interior dimensions were marked by ballpoint pen and they were 1-2 millimetres offset in order to have a safe margin of error and also because the cutting machine always eat some thickness. The excess will be easily polished after.

To prepare the piece 4 holes were drilled, this will allow the saw tool to cut from one hole to the next. The holes should be large enough to allow the blade to enter and move, but a large hole drilled at once can damage the piece and cause it to split. We will then make a pilot hole which is a smaller hole drilled before a screw is inserted or a larger hole. This technique prevents the material from splitting.

The size of the pilot drill bit is 6 mm and the next bit is 10mm, it will rest on top of the pilot hole which will guide it through the material. The result is showed in figures 4.2 and 4.3.

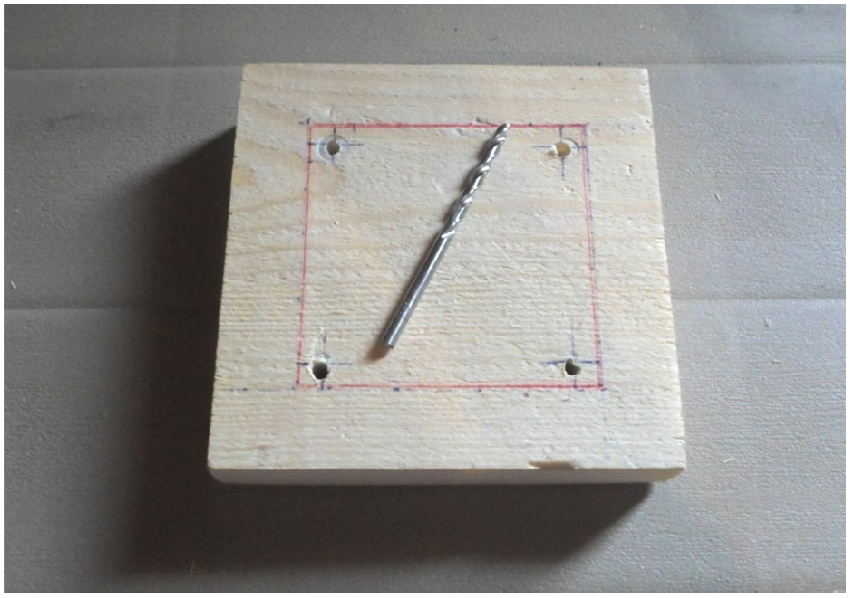

Figure 4.2 Pilot holes and pilot drill bit.

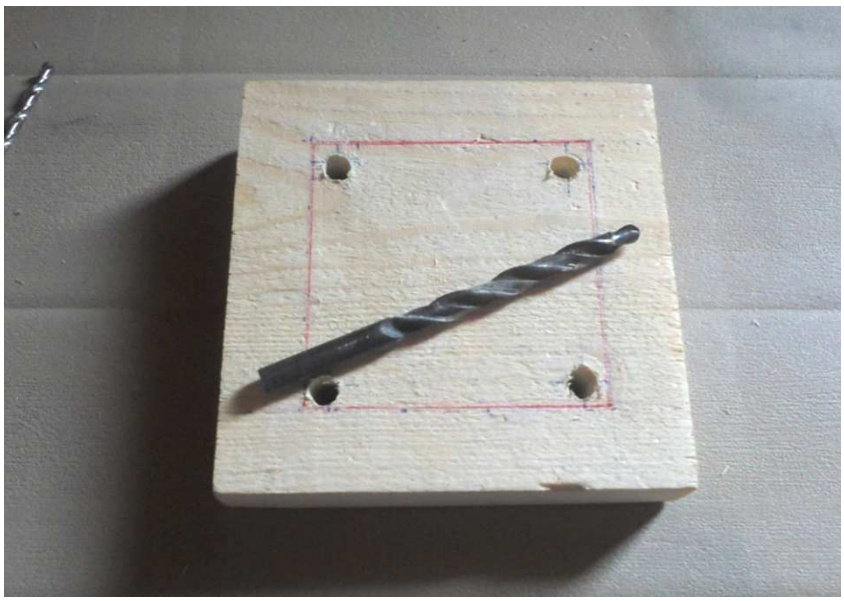

Figure 4.3 Holes that allow material cutting.

After removing the material, 4 holes were drilled on each side to form the attachment point for the arms. After that some careful polishing was done to remove any irregularities and to smoothen the surfaces. Finally, were formed on the inside and outside faces to remove sharp edges, both for safety and to give an aesthetic look.

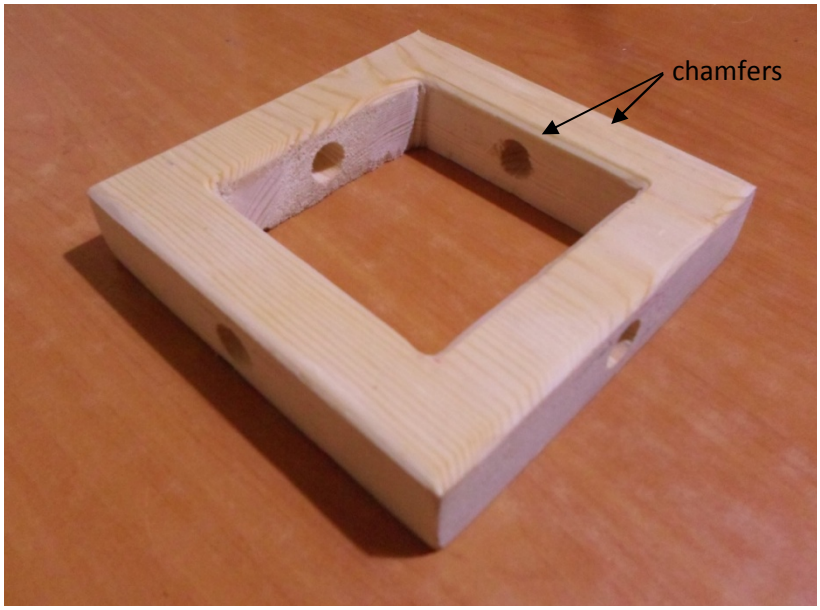

Figure 4.4 Central square after finishing.

4.3 The arms

The four arms are showed in figure 4.4, they will be rounded in one end to fit in the main frame.

Figure 4.5 Arms of the quadcopter.

4.4 Landing gear

We will use plastic covers as landing gears, they will be mounted on a plastic plate that attaches to the main frame. Plastic is both a light material and a good absorber. This landing gear will give height and clearance to the quadcopter parts while on the ground and absorb the shock when it lands.

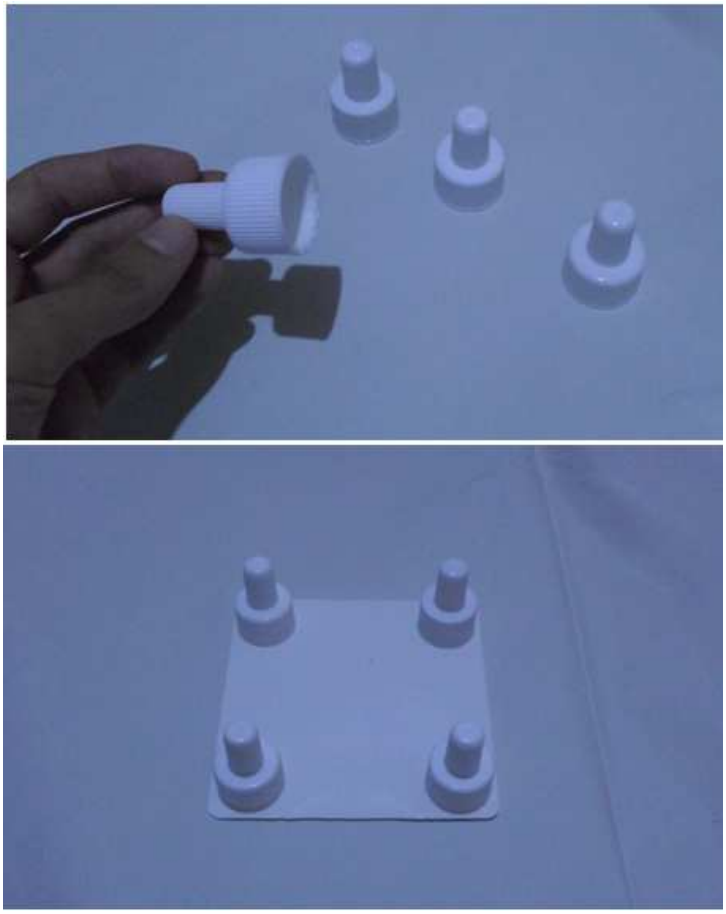

Figure 4.6 Landing gear.

4.5 Assembling and finishing

In this step the arms are attached to their places using wood adhesive (figure 4.7). The plastic covers were attached to the plate using pressure and also super glue. The entire landing gear was attached to the frame by small screws.

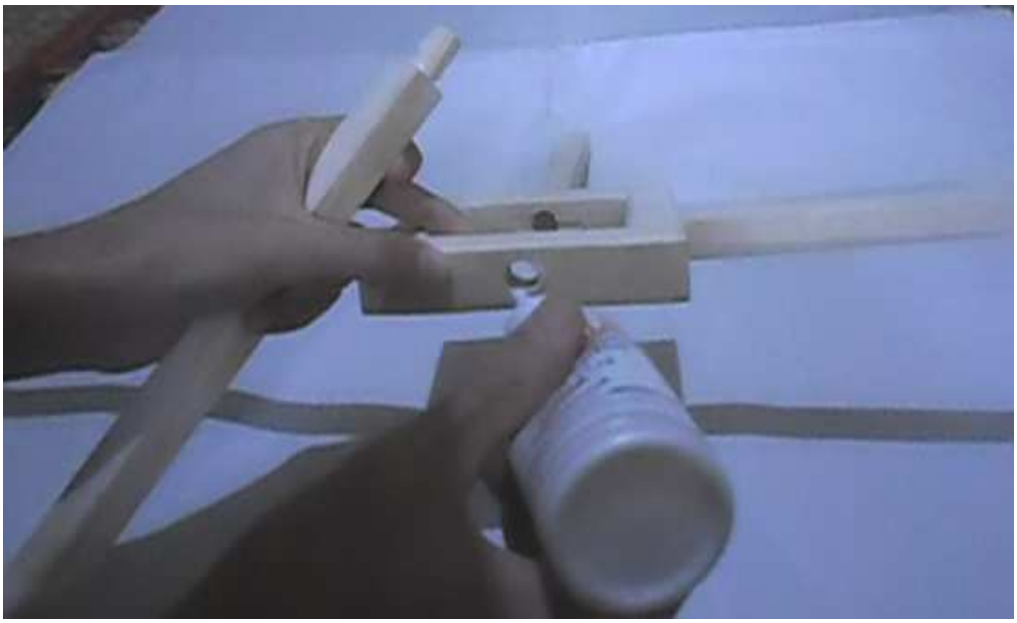

Figure 4.7 Attaching by glue.

Finally, our quadcopter is completed:

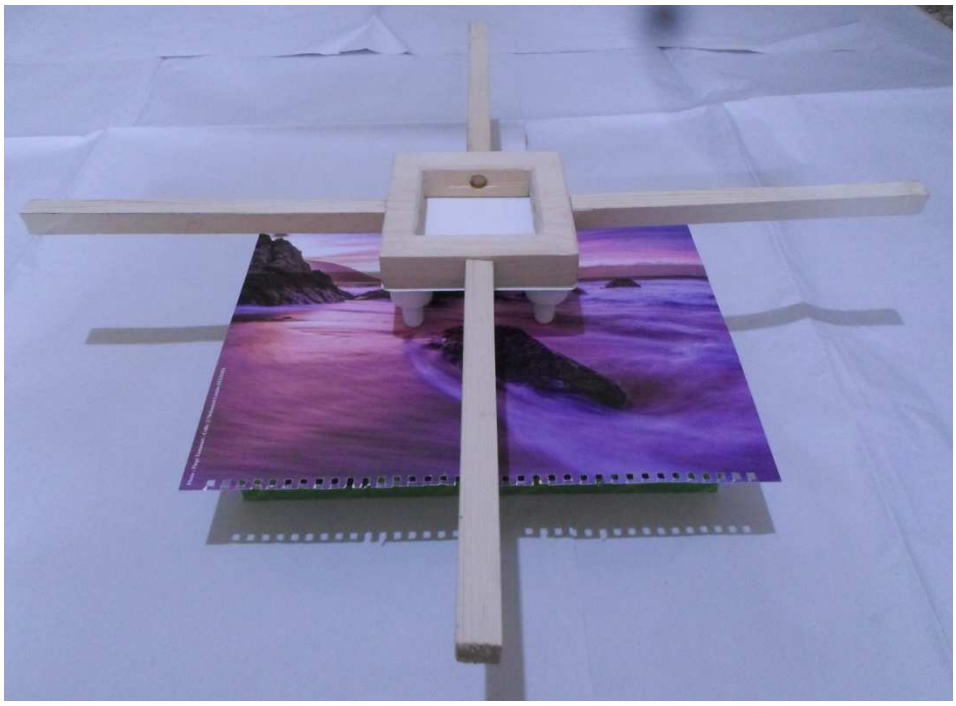

4.8 Final quadcopter.

Appendix A

A.1 Euler angles

The ZYX sequence of rotations is given as follows [26]: The airplane is imagined first to be oriented so that F_b axes are parallel to those of F_e (see figure A.1), and then the following rotations are applied:

1. A rotation around the z_e (yaw-axis) for an angle of ψ for the intermediate position $x_1y_1z_1$, (z_1=z_e).

2. A rotation around the new y-axis, y_1 (pitch-axis) for an angle of θ, to the intermediate position $x_2y_2z_2$ ($y_2 = y_1$).

3. Rotation around the new x-axis, $x_b = x_2$ (roll-axis) for an angle of ϕ, to the final position $x_by_bz_b$.

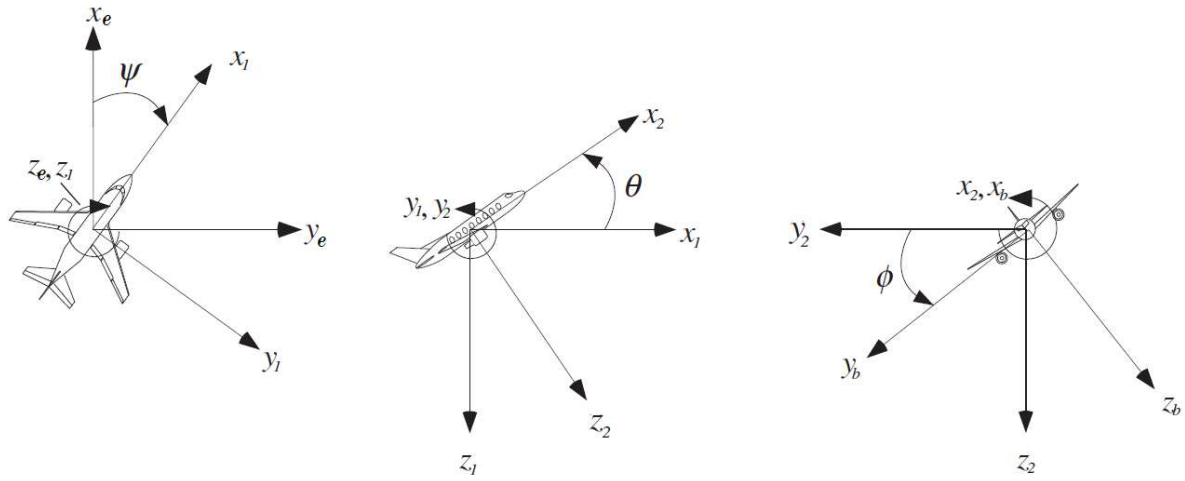

Figure A.1 Euler sequence of rotations used in aerospace.

Based on the rotations and axes conventions above, the yaw angle ψ is the angle between north and the projection of the aircraft longitudinal axis onto the horizontal plane, the pitch angle θ is the angle between the aircraft longitudinal axis and horizontal, and the roll angle ϕ represents a rotation around the aircraft longitudinal axis after rotating by yaw and pitch.

Each elementary rotation is expressed by a transformation matrix:

Yaw rotation (ψ) about z_e axis:

$$\begin{bmatrix} x \\ y \\ z \end{bmatrix}_1 = \begin{bmatrix} \cos\psi & \sin\psi & 0 \\ -\sin\psi & \cos\psi & 0 \\ 0 & 0 & 1 \end{bmatrix} \begin{bmatrix} x \\ y \\ z \end{bmatrix}_e \qquad \text{(A.1)}$$

Pitch rotation (θ) about y_1 axis:

$$\begin{bmatrix} x \\ y \\ z \end{bmatrix}_2 = \begin{bmatrix} \cos\theta & 0 & -\sin\theta \\ 0 & 1 & 0 \\ \sin\theta & 0 & \cos\theta \end{bmatrix} \begin{bmatrix} x \\ y \\ z \end{bmatrix}_1 \tag{A.2}$$

Roll rotation (ϕ) about x_2 axis:

$$\begin{bmatrix} x \\ y \\ z \end{bmatrix}_b = \begin{bmatrix} 1 & 0 & 0 \\ 0 & \cos\phi & \sin\phi \\ 0 & -\sin\phi & \cos\phi \end{bmatrix} \begin{bmatrix} x \\ y \\ z \end{bmatrix}_2 \tag{A.3}$$

The transformation matrix $\boldsymbol{R}_e^b$ that transforms from F_e to F_b is the product of the 3 single-rotation matrices. We note here that the order is inversed, because in every single transformation we pre-multiply by the transformation matrix, if we substitute (A.1) in (A.2) and then in (A.3) we get:

$$[\boldsymbol{R}_e^b(\phi,\theta,\psi)] = \left[\, \boldsymbol{R}_E^1(\psi)\, \boldsymbol{R}_1^2(\theta)\boldsymbol{R}_2^B(\phi)\right]$$

$$= \begin{bmatrix} 1 & 0 & 0 \\ 0 & \cos\phi & \sin\phi \\ 0 & -\sin\phi & \cos\phi \end{bmatrix} \begin{bmatrix} \cos\theta & 0 & -\sin\theta \\ 0 & 1 & 0 \\ \sin\theta & 0 & \cos\theta \end{bmatrix} \begin{bmatrix} \cos\psi & \sin\psi & 0 \\ -\sin\psi & \cos\psi & 0 \\ 0 & 0 & 1 \end{bmatrix}$$

$$= \begin{bmatrix} \cos\theta\cos\psi & \cos\theta\sin\psi & -\sin\theta \\ -\cos\phi\sin\psi + \sin\phi\sin\theta\cos\psi & \cos\phi\cos\psi + \sin\phi\sin\theta\sin\psi & \sin\phi\cos\theta \\ \sin\phi\sin\psi + \cos\phi\sin\theta\cos\psi & -\sin\phi\cos\psi + \cos\phi\sin\theta\sin\psi & \cos\phi\cos\theta \end{bmatrix} \tag{A.4}$$

For example:

$$\boldsymbol{g}_b = [\, \boldsymbol{R}_2^b \boldsymbol{R}_1^2 \boldsymbol{R}_e^1\,]\boldsymbol{g}_e = \boldsymbol{R}_e^b \boldsymbol{g}_e \tag{A.5}$$

Where $\boldsymbol{g}_b$ and $\boldsymbol{g}_e$ are both the gravity vector, but expressed in body frame and Earth frame respectively .

A.2 Aircraft angular rates and Euler rates

Gyroscopes mounted on board of the aircraft measure angular rates (also called angular velocities) about the x_b, y_b, and z_b axes, i.e. in the body frame, these angular rates are referred to by the vector $\boldsymbol{\Omega} = [p\ q\ r]^T$. This means that the derivatives of our Euler Angles rates $\dot{\boldsymbol{\eta}} = \left[\dot{\phi}\ \dot{\theta}\ \dot{\psi}\right]^{\mathrm{T}}$ are not what is being reported by the rate gyroscopes. And because roll, pitch, and yaw each occur in different frames (inertial frame, intermediate frame 1 and intermediate frame 2, see figure A.1), each gyro angular rate output must be converted to a different coordinate frame in order to get Euler angles rates [34].

The resulting transformation matrix which is used to convert body-frame angular rates to Euler angular rates is given by:

$$\boldsymbol{D}(\psi, \theta, \phi) = \begin{bmatrix} 0 & \sin\phi/\cos\theta & \cos\phi/\cos\theta \\ 0 & \cos\phi & -\sin\phi \\ 1 & sin\phi\tan\theta & \cos\phi\tan\theta \end{bmatrix} \tag{A.6}$$

Note that this transformation matrix, unlike $\boldsymbol{R}$, is not orthogonal

The Euler Angle rates can be then computed as:

$$\dot{\boldsymbol{\eta}} = \boldsymbol{D}\,\boldsymbol{\Omega} \tag{A.7}$$

$$\begin{bmatrix} \dot{\psi} \\ \dot{\theta} \\ \dot{\phi} \end{bmatrix} = \begin{bmatrix} 0 & \sin\phi/\cos\theta & \cos\phi/\cos\theta \\ 0 & \cos\phi & -\sin\phi \\ 1 & sin\phi\tan\theta & \cos\phi\tan\theta \end{bmatrix} \begin{bmatrix} p \\ q \\ r \end{bmatrix}$$

Which results in:

$$\begin{bmatrix} \dot{\psi} \\ \dot{\theta} \\ \dot{\phi} \end{bmatrix} = \begin{bmatrix} q\sin\phi/\cos\theta + r\cos\phi/\cos\theta \\ q\cos\phi - r\sin\phi \\ p + qsin\phi\tan\theta + r\cos\phi\tan\theta \end{bmatrix} \tag{A.8}$$

This operation illustrates mathematically why gimbal lock occurs when using Euler Angles: there is division by $\cos\theta$ in two places of the matrix $\boldsymbol{D}$, the denominator goes to zero when the pitch angle approaches ±90 degrees and the matrix elements diverge to infinity, causing the filter of the sensor to fail [34].

Conclusion and perspectives

This work presented the modelling and design of a quadcopter platform, the results of simulation proved that extreme flight loads won't cause the rupture of the platform. We have also found that fibres orientation of the material affects greatly the state of deformation, but not the state of stress.

While this work was about quadcopter drones, it helped me to gain wider understanding of several aspects of aeronautics, such as flight mechanics and design methodology. I also had the opportunity to ameliorate my skills in CAD analysis.

In the same way I hope that this thesis helps other students in their research and that my project will become a starting point for an autonomous vehicle equipped with advanced sensors. I also hope that this structural analysis will be followed by another analysis for the entire aircraft, and if possible with a topology optimisation to improve the design.

Bibliography

[1] Quan Quan, *Introduction to multicopter design and control*. Singapore : Springer Nature Singapore, 2017.

[2] Kevin Desmond, *Electric airplanes and drones: A history*., 2018.

[3] Roberto Opromolla, Giuseppe Inchingolo, and Giancarmine Fasano, "Airborne Visual Detection and Tracking of Cooperative UAVs Exploiting Deep Learning," *Sensors*, 2019.

[4] Nikolaos Tsiamis, Loukia Efthymiou, and Konstantinos P. Tsagarakis, "A Comparative Analysis of the Legislation Evolution for Drone Use in OECD Countries," *Drone*, 2019.

[5] David Morgan. Reuters. [Online]. https://www.reuters.com/article/us-usa-drones-china-idUSKBN0N72P220150416

[6] Higinio González-Jorge et al., "Unmanned Aerial Systems for civil applications: A review," *Drones*, 2017.

[7] House of Commons, "Commercial and recreational drone use in the UK," London, UK, 2019.

[8] European Commission, "Civil Drones in Society: Societal and Ethics Aspects of Remotely Piloted Aircraft Systems," Luxembourg, 2014.

[9] (2019) ALG24. [Online]. https://www.alg24.net/bejaia-arrestation-dun-individu-possession-drones-equipes-cameras/

[10] (2019) Liberté. [Online]. https://www.liberte-algerie.com/actualite/saisie-dun-drone-a-ain-temouchent-329939

[11] Claudia Stöcker, Rohan Bennett, Francesco Nex, Markus Gerke, and Jaap Zevenbergen, "Review of the Current State of UAV Regulations," *Remote sensing*, 2017.

[12] DJI. (2019) DJI Improves Geofencing To Enhance Protection of European Airports and Facilities. [Online]. https://www.dji.com/newsroom/news/dji-improves-geofencing-to-enhance-protection-of-european-airports-and-facilities

[13] United States Forest Service. If You Fly, We Can't. [Online]. https://www.fs.usda.gov/managing-land/fire/uas/if-you-fly

[14] PwC, "Clarity from above: PwC global report on the commercial applications of drone technology," 2016.

[15] "The agri culture," *Drones magazine*, no. 25, 2017.

[16] DroneDeploy. (2017) https://blog.dronedeploy.com/drones-in-agriculture-then-and-now-ebde3df01667.

[17] FAO, "E-Agriculture in action: Drones for agriculture," 2018.

[18] Lina Tang and Guofan Shao, "Drone remote sensing for forestry research and practices," *Journal of Forestry Research*, 2015.

[19] Claire Burke, Paul R. McWhirter, Josh Veitch-Michaelis, and Owen McAree, "Requirements and Limitations of Thermal Drones for Effective Search and Rescue in Marine and Coastal Areas," *drone*, 2019.

[20] Royal Aeronautical Society. Life saving drones. [Online]. https://www.aerosociety.com/news/life-saving-drones/

[21] Muhammad Arsalan Khan et al, "UAV-Based Traffic Analysis: A Universal Guiding Framework Based on Literature Survey," *Transportation Research Procedia*, 2017.

[22] Lee Ann Shay. (2020) Aviation Week Network. [Online]. https://aviationweek.com/shows-events/mro-americas/aar-plans-becoming-digital-company

[23] Airbus. www.airbus.com.

[24] Luis Rodolfo García Carrillo, Alejandro Enrique Dzul López, Rogelio Lozano, and Claude Pégard, *Quad Rotorcraft Control: Vision-Based Hovering and Navigation*.: Springer-Verlag, 2013.

[25] Abhijit Das, Frank Lewis, and Kamesh Subbarao, "Backstepping Approach for Controlling a Quadrotor Using Lagrange Form Dynamics," *Journal of Intelligent and Robotic Systems*, 2009.

[26] BERNARD ETKIN and LLOYD DUFF REID, *Dynamics of Flight: stability and controle*.: John Wiley and Sons, 1996.

[27] Brescianini Dario, Hehn Markus, and D'Andrea Raffaello, "Nonlinear Quadrocopter Attitude Control," 2013.

[28] MALCOLM J. ABZUG and E. EUGENE LARRABEE, *Airplane Stability and Control*.: Cambridge University Press, 2002.

[29] Samir BOUABDALLAH, *Doctoral thesis: design and control of quadrotors with application to autonomous flying*.: ÉCOLE POLYTECHNIQUE FÉDÉRALE DE LAUSANNE, 2007.

[30] Eric N. Landis, Ian Smith, and Eric Landis, "Finite element techniques and models for wood fracture mechanics," *Wood Science and Technology*, 2004.

[31] R. F. S. Hearmon, *The elasticity of wood and plywood.*: H.M. Stationery office, 1948.

[32] Ali H.Nayfeh and P. Frank Pai, *Linear and nonlinear structural mechanics*. Weinheim: WILEY-VCH Verlag, 2004.

[33] US Forest products laboratory, "Chapter 09: Structural Analysis Equations," in *Wood Handbook*.

[34] CH Robotics LLC. [Online]. http://www.chrobotics.com/library/understanding-euler-angles